Diagnosing water variations within the Amazon basin using satellite data

M. Azarderakhsh, W. B. Rossow, F. Papa, H. Norouzi, R. Khanbilvardi

Diagnosing water variations within the Amazon basin using satellite data

Marzieh Azarderakhsh,[1,2] William B. Rossow,[2] Fabrice Papa,[2,3] Hamidreza Norouzi,[2,4] and Reza Khanbilvardi[2]

Received 12 April 2011; revised 14 October 2011; accepted 14 October 2011; published 21 December 2011.

[1] The components of the Amazon water budget and their spatiotemporal variability are diagnosed using monthly averaged remote sensing-based data products for the period September 2002-December 2006. The large Amazon basin is divided into 14 smaller watersheds, and for each of these sub-basins, fresh water discharge is estimated from the water balance equation using satellite data products. The purpose of this study is to learn how to apply satellite data with global coverage over the large tropical regions; therefore several combinations of remote sensing estimates including total water storage changes, precipitation and evapotranspiration. The results are compared to gauge-based measurements and the best spatiotemporal agreement between estimated and observed runoff is within 1 mm/d for the combination of precipitation from the GPCP and the Montana evapotranspiration product. Mean annual precipitation, evapotranspiration and runoff for the whole basin are estimated to be 6.3, 2.27 and 3.02 mm/d respectively but also show large spatial and temporal variations at sub-basin scale. Using the most consistent data combination, the seasonal dynamics of the water budget within the Amazon system are examined. Agreement between satellite based and in situ runoff is improved when lag-times between sub-basins are included (RMSE from 0.98 to 0.61 mm/d). We estimate these lag times based on satellite-inferred inundation extents. The results reveal not only variations of the basin forcing but also the complex response of the inter-connected sub-basin (SB) water budgets. Inter-annual and inter-SB variation of the water components are investigated and show large anomalies in northwestern and eastern downstream SBs; aggregate behavior of the whole Amazon is more complex than can be represented by a simple integral of the forcing over the whole river system.

Citation: Azarderakhsh, M., W. B. Rossow, F. Papa, H. Norouzi, and R. Khanbilvardi (2011), Diagnosing water variations within the Amazon basin using satellite data, *J. Geophys. Res.*, *116*, D24107, doi:10.1029/2011JD015997.

1. Introduction

[2] Understanding, characterizing and predicting the distribution and cycling of terrestrial waters are major goals of hydrology and climate research as well as major requirements for water resource management. However, seasonal and interannual variations of the water budget terms, including precipitation, evapotranspiration, runoff and surface and sub-surface water storage are still not well know, at least at regional to global scales [*Bullock and Acreman*, 2003].

[3] The Amazon basin is of special interest because, with the largest drainage area in the world, covering about 40% of South America, variations of water exchange within its watershed can have a strong regional effects on the global and tropical climate systems: the Amazon in its own right makes the largest contribution (15%–20%) to the total fresh water discharge to the global ocean. Changes in atmospheric circulation and precipitation can translate into changes in the discharge to the ocean and affect the atmospheric moisture transport from the Amazon region to adjacent regions [*Marengo*, 2005; *Espinoza Villar et al.*, 2009a, 2009b]. Moreover, internal dynamics of this drainage system is complicated by the fact that the watershed extends both north and south of the equator and, as a result, has different wet and dry seasons. In the last few years, the Amazon basin has experienced severe extreme events. For instance, in 2005 a drought that affected the western parts of the basin during the dry season was blamed for lower water levels in the central and eastern parts of the river system, leading to serious effects on human activity and the biosphere and also to higher sea surface temperature (SST) in the tropical North

[1]Graduate Center, City University of New York, New York, New York, USA.
[2]NOAA-Cooperative Remote Sensing Science and Technology Center, City University of New York, New York, New York, USA.
[3]IRD LEGOS, Toulouse, France.
[4]Construction Management and Civil Engineering Technology, New York City College of Technology, New York, New York, USA.

0148-0227/11/2011JD015997

Atlantic by up to two degrees Celsius [*Marengo et al.*, 2008; *Zeng et al.*, 2008]. In 2009, the Amazon basin was hit by large and severe flooding with the central and northern regions experiencing their worst flooding in over half a century [*Chen et al.*, 2010].

[4] Large-scale water-budget studies for the Amazon basin have been conducted since the late 1970s using different techniques and atmospheric data sets from radiosondes to global reanalysis [*Costa and Foley*, 1997; *Leopoldo et al.*, 1987; *Roads et al.*, 2002; *Vörösmarty et al.*, 1996]. All these studies have emphasized the importance of remote forcing on the variations of the components of the local water budget. Several studies also investigated the closure of the terrestrial water budget and/or estimated river discharge is the Amazon using in situ gauge streamflow measurements together with a simple water balance equation method ($R = P-ET-\Delta S$, where R = runoff, P = precipitation, ET = evapotranspiration and ΔS = total water storage changes), or hydrological modeling forced with meteorological observations, numerical simulations or a combination of remote sensing-based water height estimates and height-discharge relations [*Coe et al.*, 2002; *Decharme et al.*, 2008]. Some studies have tried to close the water budget at basin scale or estimate discharge from the water balance equation and have reported large uncertainties in the estimated discharge due to the errors in the individual components of the water budget [*Coe et al.*, 2002; *Getirana et al.*, 2010; *Marengo*, 2005; *Sheffield et al.*, 2009; *Syed et al.*, 2009, 2005; *Tang et al.*, 2010; *Zeng*, 1999]. Because of the need to calibrate hydrological models to specific locations and their relatively low spatial resolution (global or continental or large basin scales), applying these models to the Amazon basin with complicated rainfall and evapotranspiration variability is not always accurate [*Getirana et al.*, 2010].

[5] There are different studies on quantifying the water budget components, each trying different methodologies. However, they give different estimates that make the accurate estimate of these components difficult and that will be discussed here.

[6] Gauge-based estimates of global and continental freshwater discharge are limited by geographic and political restrictions due to institutional and economic constraints. Existing regional networks are usually located in more affluent countries. Quantifying freshwater discharge into the ocean is further complicated by the fact that existing stream gauges are often located far from the point of inflow into the ocean [*Dai and Trenberth*, 2002]. Also because of technological, economical and institutional limitations, the number of gauging stations and access to river discharge information have been declining since 1980 [*Bjerklie et al.*, 2003]. Even though discharge is an accurate measure of integrated terrestrial runoff, it typically offers little information about the spatial distribution of runoff within a watershed unless the river basins are highly instrumented. Therefore, disaggregation of the river runoff is necessary when spatially distributed runoff information is needed especially in large and complex basins like Amazon [*Fekete et al.*, 2002].

[7] The surface and upper-air observational network in the Amazon region is very sparse and, by itself, cannot provide the comprehensive meteorological information needed to accurately drive numerical models to estimate water-balance. Therefore, imperfect models or products from data assimilation or gridded reanalyses and rainfall data sets have been used to make these estimates [*Marengo*, 2005]. The National Centers for Environmental Prediction (NCEP), European Centre for Medium Range Weather Forecasts (ECMWF) and National Aeronautics and Space Administration/Data Assimilation Office (NASA/DAO), NASA/Goddard Earth Observation System (GEOS) have developed analysis projects using different global atmospheric models with land-surface physics and data assimilation to characterize features of the terrestrial water budget. However, the level of uncertainty in these estimates of the components of the water budget is not yet well determined [*Marengo*, 2005; *Roads et al.*, 2002].

[8] The spatiotemporal variations of precipitation globally and over the Amazon basin have been analyzed in several studies using remote sensing techniques [*Gu et al.*, 2007; *Huffman et al.*, 2009, 2007; *Joyce et al.*, 2004], rain gauge based measurements [*Espinoza Villar et al.*, 2009a, 2009b], a combination of these methods and from climatology. Although the satellite-based estimates are not able to capture the extreme rainfall rates reliably [*AghaKouchak et al.*, 2011a, 2011b] they can be used to study the seasonal variability of precipitation. [*Espinoza Villar et al.*, 2009a, 2009b] investigated the seasonal and interannual variations of rainfall over different parts of the basin using rain gauge measurements and reported a clear contrast in the annual phase between northern and southern regions in austral summer (December–January–February, DJF) and austral winter (June–July–Aug, JJA), as well as a systematic decrease of mean rainfall rate since 1983 at −0.32% per decade.

[9] Evapotranspiration is estimated from reanalysis models including NCEP-DOE AMIP-II reanalysis (R-2) [*Kanamitsu et al.*, 2002], European Centre for Medium-Range Forecasts (ECMWF), ERA-40 [*Gibson et al.*, 1997], from the empirical Penman-Monteith formulation [*Monteith*, 1965] using different remote sensing data to quantify net surface radiation and surface meteorology inputs [*Mu et al.*, 2007; *Sheffield et al.*, 2010], using model simulations with radiation and meteorological forcing, or employing a water balance residual approach ($P-R-\Delta S$) [*Rodell et al.*, 2004; *Sheffield et al.*, 2010]. [*Jimenez et al.*, 2011] compared twelve different global evapotranspiration estimates and showed that the largest absolute disagreements occur over tropical rain forest regions. These differences may be due to difference in inputs to the estimates, such as the net radiation, vegetation and meteorological data, or to differences in physics, including whether evaporation from intercepted precipitation or open water on the surface is accounted for.

[10] The total terrestrial water storage is the sum of the amounts of snow, soil moisture, surface and sub-surface water; changes in storage can now be estimated using the Gravity Recovery and Climate Experiment (GRACE) measurements [*Wahr et al.*, 2004]. Discharge or surface water volume changes have been estimated using altimetry data and height-volume ratios [*Alsdorf et al.*, 2007; *Alsdorf*, 2003; *Alsdorf and Lettenmaier*, 2003; *Frappart et al.*, 2008], surface water areas using multisatellite techniques [*Papa et al.*, 2008b, 2010; *Prigent et al.*, 2007] and "direct" gauge measurements [*Espinoza Villar et al.*, 2009a, 2009b].

[11] This study aims to investigate seasonal and interannual variations of the individual water balance (WB) components and their interactions. For this we investigate

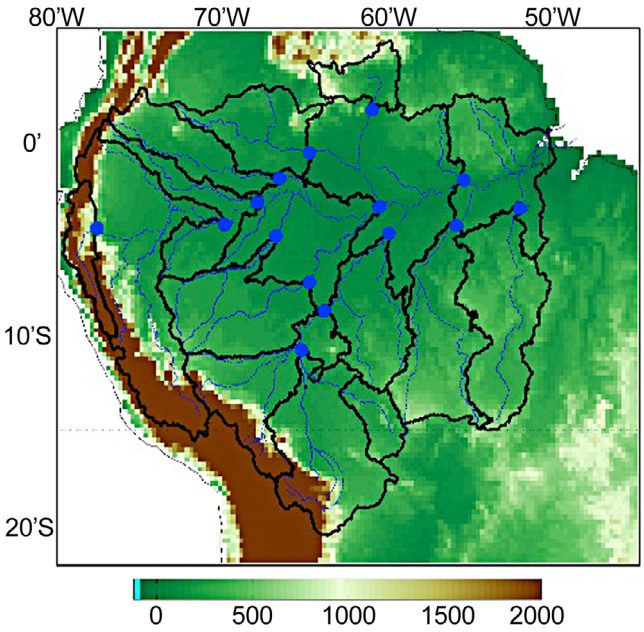

Figure 1. Delineation of the Amazon and its SBs at different gauges using SRTM topography data.

the use of different satellite data products over the Amazon, including estimates of precipitation, evapotranspiration, together with water storage changes, to infer the runoff term as a residual from the water balance equation. Results are compared and evaluated with in situ discharge measurements. In order to better understand the dynamics of each component and their interactions, the Amazon basin is studied as a whole and also divided into smaller sub-basins (SBs) to determine the most consistent combination of data products for quantifying the seasonal and interannual variations of water budget components in all individual SBs. The best data combination is selected based on the best consistency in representing the spatial and temporal variability of estimated runoff compared to observed runoff. The dynamics of the water budget components and their interactions are then investigated at inter-basin and seasonal scales.

[12] Section 2 defines the study area and the different data sets that are used. The spatiotemporal variability over the SBs from each data product is described. Section 3 presents estimates of the runoff as a residual from the water balance equation for different precipitation and evapotranspiration data combinations along with an indication of their uncertainties. Section 4 explains the choice of the most consistent data combination from the results of Section 3 by comparison of the estimated and observed runoff for the SBs. The best precipitation and evapotranspiration data combination is the Global Precipitation Climatology Project (GPCP) precipitation and the evaporation estimates of the University of Montana. The agreement between satellite based and in situ runoff is significantly improved by using satellite based inundation extent verifications to estimate lag-times between SBs. Section 5 uses this data combination to characterize the seasonal and inter-annual dynamics of the water budget components and their interactions; especially the interactions among the SBs. Finally, Section 6 gives the summary and conclusions.

2. The Amazon Basin and Its SBs: Data Sets and Analysis of the Different Products

2.1. Region of Interest

[13] The Amazon is the world's largest drainage system with a total area of 6×10^6 km^2 carrying 15–20% of the global fresh water to the ocean [*Richey et al.*, 1986]. Due to its size and its position astride the Equator, the Amazon basin exhibits very complicated rainfall, evapotranspiration and runoff patterns; within its boundaries, the interactions of its many SBs make it a very interesting dynamic system.

[14] In this study we consider the entire Amazon basin as well as 15 SBs (Figure 1). We selected these 15 SBs based on a careful analysis of the availability of in situ stations (at the outlet of each SB) that give their daily discharge data, their location in the basin, data periods, drainage area and mean discharge (Figure 1 and Table 1). These SBs show drainage areas ranging from 117,000 km^2 (SB 1) to 761,500 km^2 (SB 2, Table 1). Following [*Espinoza Villar et al.*, 2009a, 2009b] the geographic extents of the main basin and SBs were estimated using ArcGIS and the Shuttle Radar Topography Mission (SRTM) Digital Elevation Model [*Rabus et al.*, 2003] with a resolution of 3 arc sec and checks with SBs generated by the Environmental Research Observatory (ORE) Geodynamical, hydrological

Table 1. Situation, Mean (Qmean), Minimum (Qmin) and Maximum (Qmax) Runoff of SBs (mm/d)

Basin Number	Station	River	Lat	Lon	Area (km^2)	Qmean	Qmax	Qmin
1	Borja	Maranon	−4.43	−77.6	117000	3.65	6.28	1.79
2	Tabatinga	Amazonas	−4.25	−69.93	745300	3.39	5.33	1.24
3	St-Antonio Do Ica	Solimoes	−3.08	−67.93	263000	6.83	11.46	1.93
4	Acanaui	Japura	−1.82	−66.6	251500	4.79	8.31	1.47
5	Serrinha	Negro	−0.48	−64.83	287200	5.06	9.29	1.32
6	Caracarai	Branco	1.83	−61.38	134200	2.14	7.04	0.21
7	Labrea	Purus	−7.25	−64.8	165000	2.07	4.16	0.31
7	Gaviao	Jurua	−4.84	−66.85	258000	1.14	2.74	0.2
8	Guayaramerin	Mamore	−10.8	−65.3	512300	1.68	4.19	0.02
9	Porte Velho	Madeira	−8.74	−63.92	490100	2.59	6.72	−0.17
10	Fazenda Vista Alegre	Madeira	−4.68	−60.03	312900	4.37	7.79	0.2
11	Manacapuru	Sloimoes	−3.31	−60.61	435600	2.88	7.31	−0.87
12	Obidos	Amazon	−1.93	−55.5	706600	2.38	5.57	0.45
13	Itaituba	Tapajos	−4.28	−55.58	441000	1.54	5.12	0.18
14	Altamira	Xingu	−3.38	−52.14	474800	3.02	6.28	1.79
15	Outlet	Amazon			415000			

and biogeochemical control of erosion/alteration and material transport in the Amazon basin (HYBAM) Program (http://www.ore-hybam.org).

[15] SB 1 is located at the westernmost (upstream) end of the Amazon system and includes part of Andes mountains with very large rainfall variability. SBs 2 and 3 also include part of the Andes in the northwestern part of the Amazon and contain the upper portions of the Amazonas and Salimoes rivers. SBs 4, 5 and 6 carry water into the Japuru, Negro and Branco rivers in the northern part of the Amazon and make the largest contribution of water to total flow despite their smaller area. SB 7 is composed of two smaller rivers, the Purus and Jurua, in the midwestern part of the Amazon and both flow into SB 11, the Solimoes River. SB 8, the Mamore River, is in the southern part of the Amazon flowing into SB 9 and eventually 10, the Madeira River. SBs 11, Solimoes, and 12, the Amazon River proper, are in the rain forest part of the Amazon with the largest inundated areas. SB 13, the Tapajos River, and 14, the Xingu River, are in the eastern part of the Amazon and have lower rainfall variability but larger drainage areas.

2.2. Data Sets and Analysis of the Inputs

2.2.1. Topography

[16] The Shuttle Radar Topography Mission (SRTM) Digital Elevation Model (DEM) [*Rabus et al.*, 2003] data are used to delineate the geographic extents of the main basin and its SBs (Figure 1). This information with a resolution of 3 arc sec is used in Arc-GIS to generate watershed boundaries for each runoff gauge and to compute the basin slope and drainage area. Since topography data do not include information from the bottom of the river channel, it is necessary to add river network information to precisely locate the outlet of the SB for each gauge station. The river network data is used from the ORE-HYBAM program as ancillary data to generate the watersheds.

2.2.2. Precipitation

[17] We used in this study different estimates of precipitation over the Amazon basin.

[18] 1. The Global Precipitation Climatology Project (GPCP), established in 1986 by the World Climate Research Program, provides data that quantify the distribution of precipitation over the whole globe [*Adler et al.*, 2003]. The GPCP version 2.1, which is a combined satellite-gauge (SG) product, provides monthly and pentad, global 2.5° × 2.5° gridded values of precipitation totals from 1979- present [*Huffman et al.*, 2009].

[19] 2. The TRMM MultiSatellite Precipitation Analysis (TMPA) [*Huffman et al.*, 2007] is a 3-hourly (also monthly) combined microwave-IR global 0.25° by 0.25° estimate (with gauge adjustment) starting in January 1998. We used the combined gauge-adjusted product (3B42 version 6), which is scaled to monthly gauge data.

[20] 3. The Climate Prediction Center (CPC) Morphing Technique (CMORPH) uses motion vectors derived from half-hourly 8 km (at the equator) geostationary satellite IR imagery to propagate the precipitation estimates derived from passive microwave data and produces a 3-hourly 0.25-degree product available back to December 2002 [*Joyce et al.*, 2004].

[21] 4. The Precipitation Estimation from Remotely Sensed Information using Artificial Neural Networks (PERSIANN) gives 0.25° by 0.25° 3-hourly global rainfall estimates using infrared satellite imagery and surface information since 2000 [*Hsu et al.*, 1997].

[22] Comparison of the different precipitation products and their mean seasonal variations for 2003–2006 is shown for 9 representative SBs, 2, 3, 5, 7, 8, 10, 11, 12 and 14 in Figure 2. Annual mean precipitation reported by these products for the entire Amazon ranges from 5.5 mm/d (TMPA) to 6.52 mm/d (PERSIANN). Spatial patterns of different satellite precipitation data sets are significantly different as previously highlighted [*AghaKouchak et al.*, 2011b]. This could have a considerable impact on the estimated runoff in this study in different SBs.

[23] The primary and calibration sensors of GPCP and TMPA are similar and as a result they show good agreement over space and time except for the SB 1, probably because the TMPA results are adjusted to the older gauge measurements of the older GPCP data (Version 1). Generally, these two gauge adjusted products give smaller estimates in wet seasons compared to CMORPH and PERSIANN, which have precipitation greater than 3.3 mm/d, (nonshaded areas in Figure 2). However, these differences are reversed in SBs 1, 3, and 6 during dry or less rainy seasons (not shown). Another difference in seasonal cycle of the precipitation products is onset of the wet season; PERSIANN and CMORPH start in SB 5, 11 and 12 from August while climatology records and GPCP and TMPA estimates start the wet season with one or two months delay. Note that the shaded area means local dry season with total monthly precipitation less that 3.3 mm/d using GPCP data since it gives closest estimates to GPCC and climatology records.

2.2.3. Evapotranspiration

[24] We use and evaluate two ET estimates that are based on the Penman-Monteith equation [*Monteith*, 1965] using different remote sensing data as inputs. The goal is to use sub-monthly data, coincident with GRACE estimates. Therefore these two estimates are chosen for this study from among other remote sensing based estimates [*Fisher et al.*, 2008; *Wang et al.*, 2010; *Zhang et al.*, 2010]: the Princeton University and University of Montana products and will be referred as ET-PRI and ET-MON (M for Mu and Z for Zhang).

[25] [*Sheffield et al.*, 2010] calculated daily estimates of ET-PRI with input radiation and meteorological data from the International Satellite Cloud Climatology Project (ISCCP) and vegetation distribution derived from the Advanced Very High Resolution Radiometer (AVHRR) products for 1984–2006 at 2.5 deg.

[26] The other data set, ET-MON-M, uses the same algorithm with different input data and gives global 8-day, 0.05-degree, estimates over 2000–2006 [*Mu et al.*, 2007]. The Beta version ET algorithm is driven with global 1 km MODIS LAI/FPAR (Leaf Area Index/Flux Photosynthetic, Version 5), MODIS land cover (Version 4), 0.05-degree global MODIS surface albedo (Version 4), and Global Modeling and Assimilation Office (GMAO) daily meteorological data. In this study, we have used their global 1 km ET/LE data from 2002 August to 2006.

[27] We also use the monthly evapotranspiration estimates provided by University of Montana, ET-MON-Z, to study inter-annual variations of ET over the Amazon (Section 5) [*Zhang et al.*, 2010]. The algorithm quantifies canopy

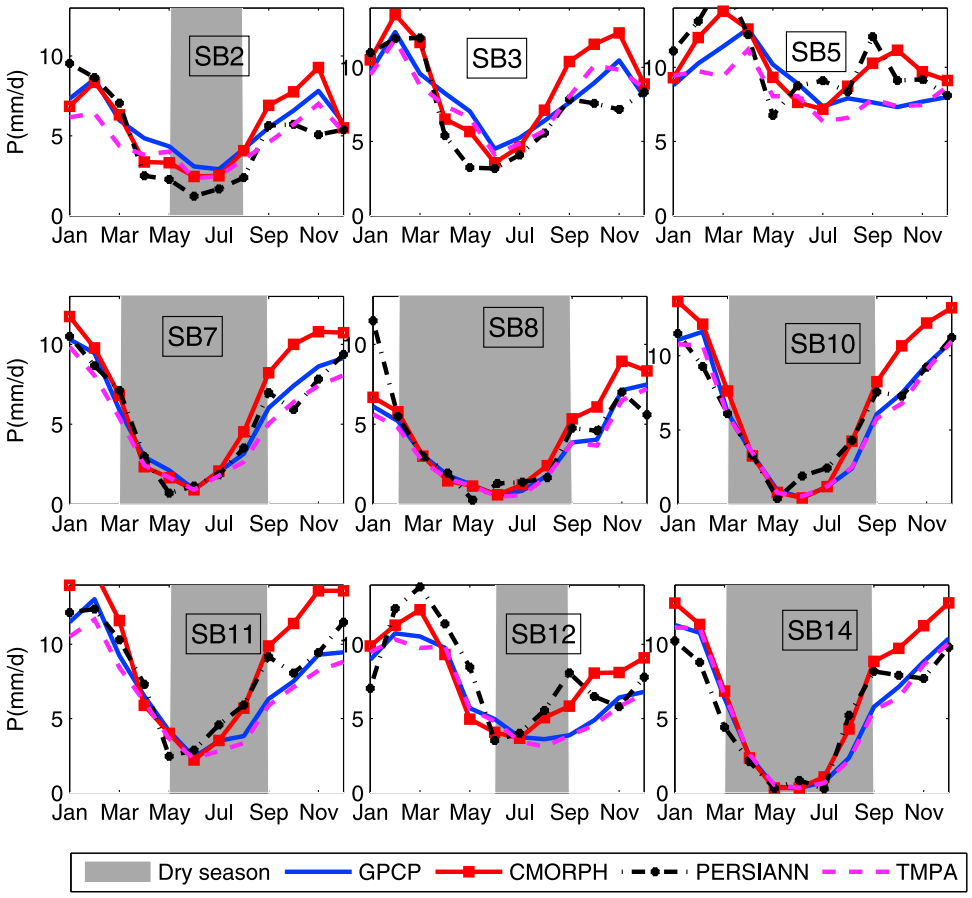

Figure 2. Seasonal variability of precipitation from different data sets for different SBs with dry seasons (P of GPCP < 3.3 mm/d) shown with shaded areas. For more information on SBs see Table 1.

transpiration and soil evaporation using a modified Penman-Monteith approach with biome-specific canopy conductance determined from the normalized difference vegetation index (NDVI) and quantifies open water evaporation using a Priestley-Taylor approach. These algorithms were applied globally using advanced very high resolution radiometer (AVHRR) Global Inventory Modeling and Mapping Studies (GIMMS) normalized difference vegetation index (NDVI) data, NCEP/NCAR Reanalysis (NNR) daily surface meteorology, and NASA/GEWEX Surface Radiation Budget Release 3.0 solar radiation inputs. This data set gives very similar values to ET-MON-M with RMS differences of up to 0.4 mm/d (RMS differences with ET-PRI is 1.03 mm/d). Therefore this ET-MON-Z and ET-PRI will be used for the interannual variations over a longer time period (1984–2006) (Section 5).

[28] Comparison of the three data sets (ET-MON-M, ET-Mon-Z, ET-PRI) is shown in Figure 3 for different SBs with their dry season shown by the shaded area. Both University of Montana products agree better with each other over different SBs than ET-PRI. The differences between ET-MON-M and ET-PRI vary among the SBs: 1 mm/d maximum mean difference (bias) between the two data sets is seen in the northern SB 6 and the 0.15 mm/d minimum difference is seen in southern SB 8. [*Getirana et al.*, 2010] used hydrological modeling and water balance for the Negro river (SB 5 and 6) for 1997–2006 to estimate annual mean, wet and dry season mean ET of 3.2, 3.5 and 2.6 mm/d respectively. The same values for ET-MON-M are 3.23, 4.1 and 2.42 mm/d and for ET-PRI they are 4.32, 5.2 and 3.33 mm/d. Note that neither data set accounts for evaporation from inundated areas even though SBs 11 and 12 have extensive and variable inundated areas [*Papa et al.*, 2008b, 2010].

[29] Open water bodies and flooded areas in the Amazon can be important contributors to ET. Evapotranspiration estimates from Princeton University, with a map grid of 2.5 degrees, are less sensitive to the inundated areas near the river. On the other hand ET-MON-Z, have finer resolution (1 km), but do not account for evaporation from flooded areas. These estimates for open water bodies are based on land cover classification maps and, therefore, do not include the effects of seasonal flooding [*Papa et al.*, 2010]. In fact, this data set shows a decrease in ET in the season with increased flooding. Also, there does not seem to be a significant increase in ET in SB 8, which contains the reservoir of the Samuel Dam. Therefore, all three ET estimates need to carefully account for the evaporation from open water areas.

[30] Generally ET exhibits small seasonal variation and decreases over the dry season due to water stress. However, ET increases during less rainy months in SBs 5, 11, 12, and 15 which have no dry season. This will be discussed more in section 5 investigating the dynamics of the water.

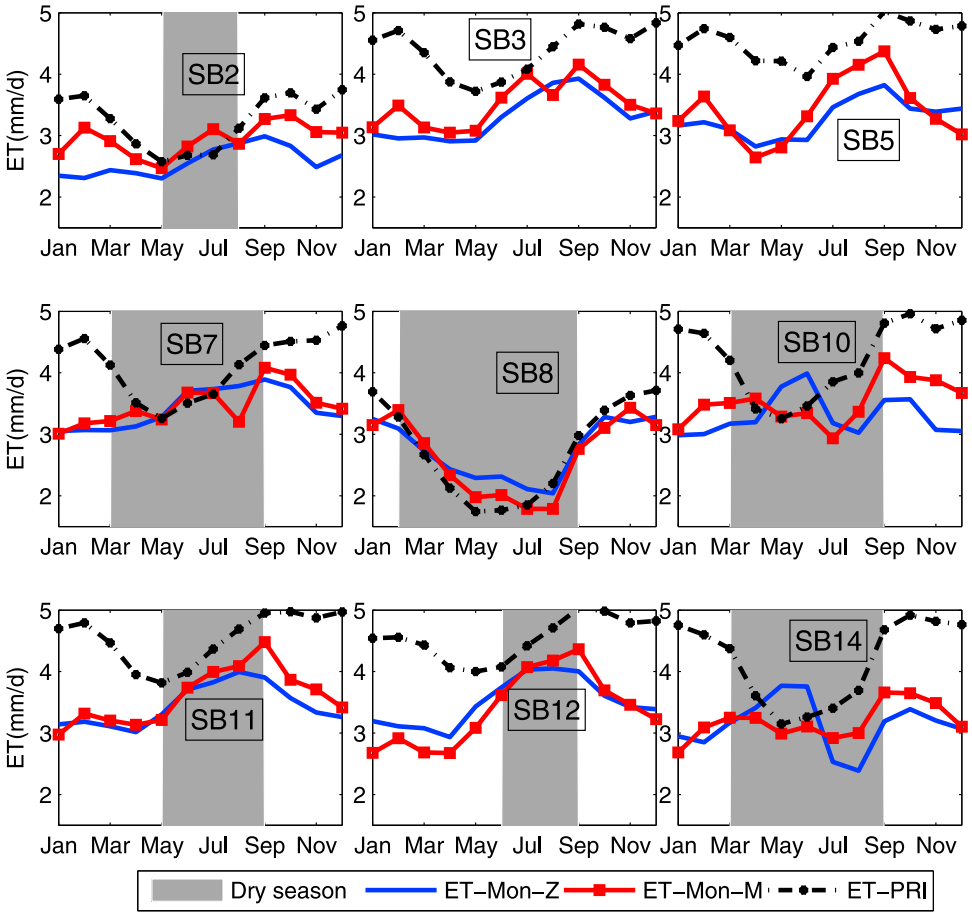

Figure 3. Seasonal variability of evaporation from different data sets for different SBs with dry seasons (P < 3.3 mm/d) shown with shaded areas. For more information on SBs see Table 1.

[31] Thus for the study of the seasonal dynamics we use ET-MON-M and for the inter-annual variation we use ET-MON-Z and ET-PRI because of their long time coverage. Although these ET estimates show different seasonal patterns over the Amazon, they agree in interannual variation exhibiting correlation coefficient of 0.98 between ET-MON-M and ET-MON-Z and 0.91 between ET-MON-M and ET-PRI.

2.2.4. Total Water Storage (TWS) Anomalies From GRACE

[32] The GRACE mission provides monthly gravity field solutions as sets of Stokes coefficients up to 1 degree at approximately 30-day intervals by measuring the distance between the two satellites since its launch in 2002. These coefficients can be used to estimate TWS changes after correction for atmospheric mass changes. We use these monthly solutions for the period from August 2002 through December 2006, except for June 2003 and January 2004 when GRACE data were unavailable.

[33] Since shorter-wavelength spherical harmonic coefficients of the gravity field have more spatial noise, smoothing is necessary to reduce it [*Seo and Wilson*, 2005]. While a large half-width can reduce the amplitude of the storage change signal, a smaller half-width can significantly decrease the signal-to-noise ratio and may even produce non-geophysical north-south stripes [*Swenson and Wahr*, 2006]. The geoid data are expressed in equivalent water height the assumption that observed gravity variations are caused by surface mass redistribution over land [*Wahr et al.*, 2004].

[34] We consider two smoothing widths to compare the signal difference in the storage changes at scales of 300 km and 500 km from the Jet Propulsion Laboratory (JPL) and Center for space research (CSR). Figure 4 shows monthly variation of the TWS obtained with these two smoothing radii for different SBs. The 500 km radius smoothes the storage changes but appears to lose some of the information as [*Swenson and Wahr*, 2006] concluded especially in downstream SBs 11 and 12. Also, the seasonal variations of the water storage changes are in better agreement with the known dry and wet seasons of the SBs except in SB 12, where the minimum occurs in the beginning of the dry season (shaded areas in Figure 4). This happens because of the coincidence of the dry season, and hence decreased runoff, from the upstream SBs discharging into this SB (5 and 11).

[35] While the analysis of the GRACE measurements can characterize terrestrial freshwater changes across a range of temporal (monthly and longer) and spatial scales (area >150,000 km^2, the lower limit of GRACE water storage detectability) [*Rodell and Famiglietti*, 1999], it cannot resolve important features of the distribution of terrestrial surface waters at higher spatiotemporal frequencies. In smaller SBs it is expected that GRACE substantially

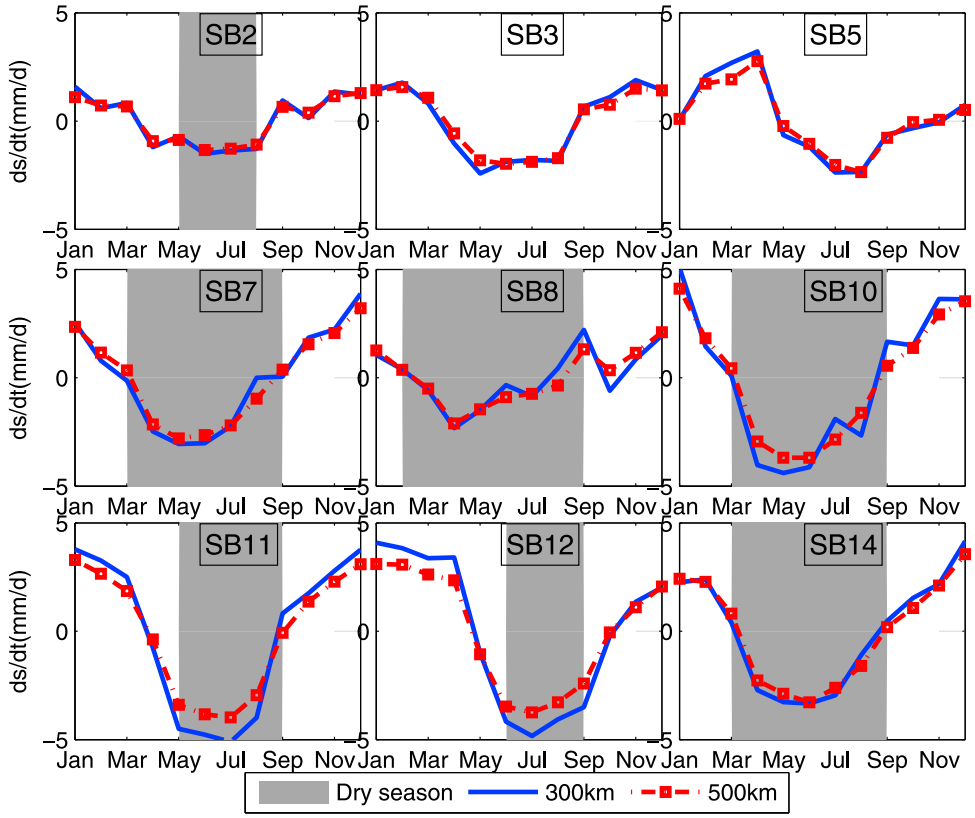

Figure 4. Seasonal variability of the water storage changes in different SBs with dry seasons (P < 3.3 mm/d) shown with shaded areas. For more information on SBs see Table 1.

underestimates the seasonal cycle of terrestrial water storage because of attenuation by the spatial smoothing [*Chen et al.*, 2007]. This was also seen in a study for the smaller Sacramento-Klamath basins with total area of 110,000 km^2 [*Tang et al.*, 2010]. In the Amazon most of the SBs have total areas >2 × 10^5 (km^2), except SB 1 which has an area of 117,000 km^2.

2.2.5. Discharge

[36] Daily water discharge data are obtained from 14 gauge stations from ORE-HYBAM program. Discharge for the downstream SBs (9, 10, 11 and 12) is computed as a residual of the total discharge of the downstream SB and the incoming discharge from upstream SBs. These values are then divided by SB area and lagged one month, as a first estimate, to be consistent with the timing of the other components of the water balance equation following [*Sheffield et al.*, 2009] in their study for Mississippi basin.

[37] Precipitation, evapotranspiration and water storage changes are averaged over each SB area. Because the observed runoff data are the total discharge at the mouth of each SB, net runoff from in-SB sources was computed as downstream minus upstream runoff. Therefore, the net runoff from SB 2 is that measured at Station 2 minus runoff from SB 1 and the net runoff from SB 3 is the total runoff from SB 3 minus that from SB 2. SB 9 obtains runoff from SB 8 and then discharges into SB 10. SB 11 collects water from SBs 3, 4 and 7 while SB 12 discharges most of its water from SBs 5, 6, 10, and 11. As seen in the Table 1 the minimum streamflow occurs in the easternmost SB 13 with a mean of 1.84 mm/d and the maximum occurs in the western SB 3 with a mean of 6.83 mm/d. We aim to investigate daily variability of the water budget components, but the coarse time resolution of GRACE data limits our initial study to monthly mean data that are used to investigate seasonal variations. Once the best precipitation and evapotranspiration combination is selected, their daily information can be used to study the water dynamics in more detail.

[38] The seasonal variation of the observed runoff is plotted in Figure 5 for different SBs along with the estimated runoff estimated runoff from water balance (the comparison of two will be discussed in section 4). Monthly variation of the observed runoff depends more on P, which has larger seasonal amplitude, than ET for most of the SBs. However, in the downstream SBs 11 and 12, net runoff has smaller seasonality because P-ET and TWS have opposite phase indicative of opposite seasonal phases for upstream SBs. SB 11 has maximum runoff in its local dry season because of abundance of stored water from upstream SBs.

2.2.6. Multisatellite Derived Inundation Data Sets

[39] A global data set of inundated area, covering the period 1993–2008, is derived by a multisatellite analysis method employing passive microwave land surface emissivities calculated from Special Sensor Microwave Imager (SSM/I) and International Satellite Cloud Climatology Project (ISCCP) observations, (ERS scatterometer measurements and AVHRR visible and near-infrared reflectances [*Papa et al.*, 2010; *Prigent et al.*, 2007]. The data set reports monthly inundated area fraction for each equal area grid cell (0.25° × 0.25° at the equator) accounting for

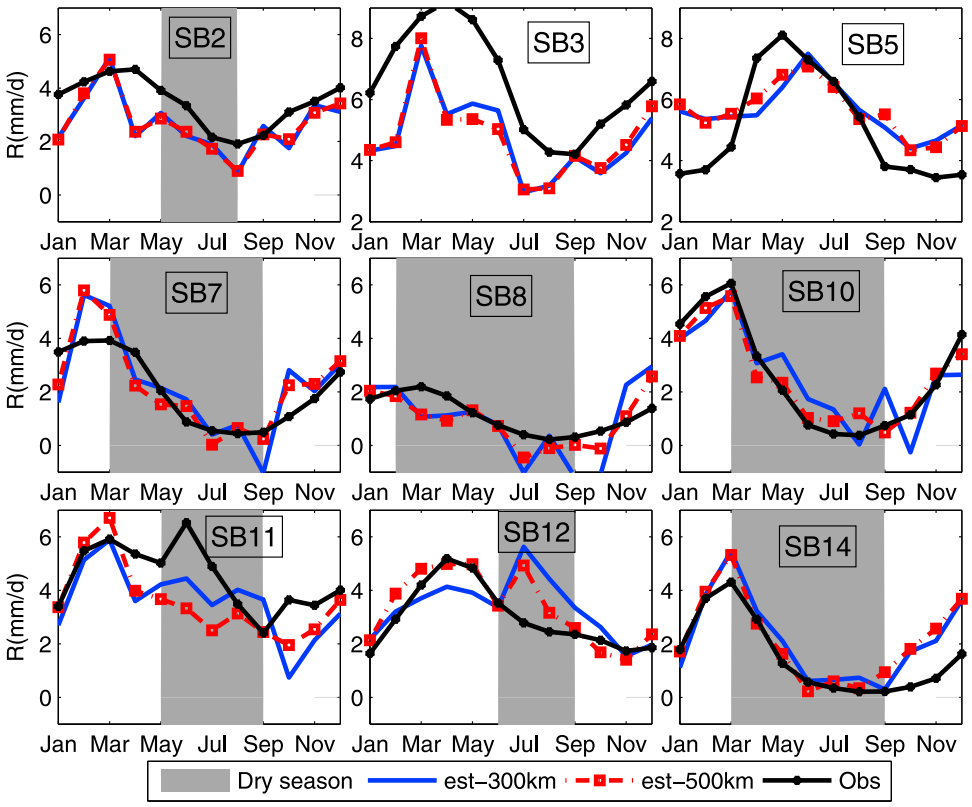

Figure 5. Monthly variation of observed runoff (solid line) and estimated using two smoothing radii for TWSC of GRACE (dashed lines) in different SBs. For more information on SBs see Table 1.

vegetation effects on the passive microwave signal of open water. The data set has been used to estimate surface water storage variations in large river basins [*Frappart et al.*, 2008, 2010] or as an indicator of runoff variation similar to the water height at the gauge station [*Papa et al.*, 2008a, 2008b]. We evaluate its ability to indicate the temporal variation of runoff to infer lag times between excess rainfall and integrated runoff at the mouth of each SB and then to the mouth of the whole Amazon.

[40] Figure 6a shows a map of the maximum annual inundation percentage difference of each map cell. Maximum inundated areas appear in the downstream SBs 11, 12 and 15 and the southern upstream SB 8. Large inundation fractions in the latter SB are due to the storage of the water in the river upstream of the Samuel dam located at the mouth of this SB.

[41] As expected from several previous studies cited above in different environments, the temporal variation of inundation exhibits a close correlation with runoff variations as illustrated here for nine representative SBs in Figure 6b. These time series will be used in Section 4 to compute the delay time for the water in upstream SBs to reach to the downstream SB instead of simply lagging one month for the whole Amazon. As seen in Figure 6b, the correlation coefficient between the time series of accumulated discharge at the outlet of each SB and its inundated fraction varies from 0.69 to 0.92, which indicates the ability of this data to detect the seasonal variation of surface water discharge.

[42] Comparing all the components shows that, generally, P is greater than ET over the whole Amazon basin, as previously deduced; but that ET exceeds P in the dry season in SBs 5, 8, 9, 10, 11 and 12. In SB 1, P is less than R, which probably indicates errors in the precipitation estimates as discussed previously. The water balance approach helps evaluate different combination of data sets for the water budget components and to understand their dynamics in Amazon basin as will be discussed in the next section.

3. Analysis Method: Estimates of Runoff and Uncertainties

[43] The terrestrial water balance for a drainage area can be written as

$$P - ET - \Delta S = R \tag{1}$$

[44] Where ΔS is the changes in terrestrial water storage (TWS) from GRACE as the difference between one monthly observation and the previous observation, P is the total precipitation (mm) for the observation month, ET is the evapotranspiration (mm) for that month, and R is the net discharge from the basin. In conventional hydrological models, the net runoff from equation (1) is estimated based on the storage in soil and groundwater, but not surface water, and then is routed in the second stage using river characteristics for the surface storage term. But GRACE data represent total water storage including the surface water. Therefore, using GRACE-based estimates of ΔS in equation (1) to determine runoff requires estimation of the travel time of the water from to the mouth of a basin.

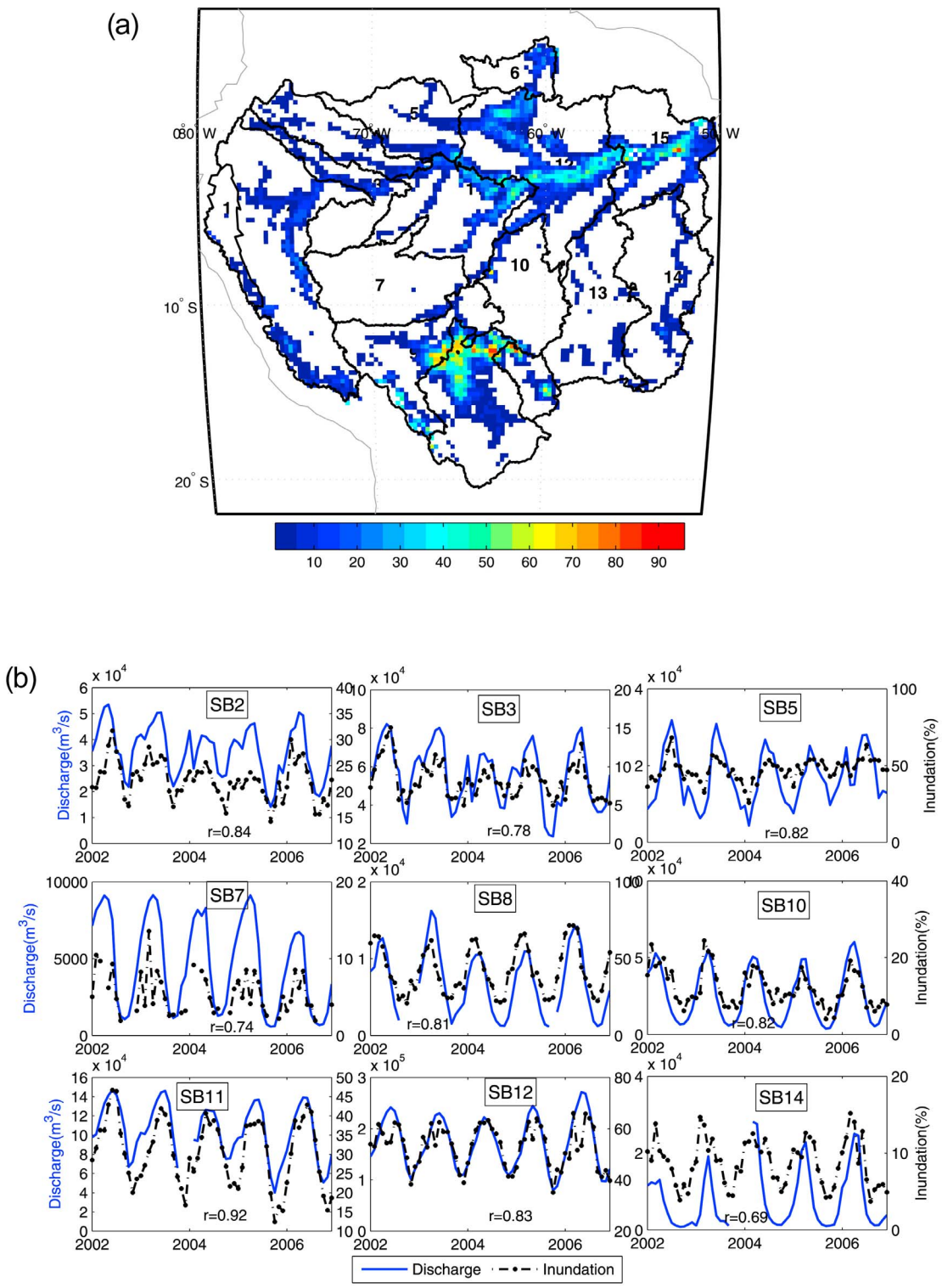

Figure 6. (a) Annual range of gridded inundation fraction (max-min) for 2003–2006. (b) Time series of inundation percentage and gauge runoff at location of gauges. Correlation coefficient for each SB is shown in each plot by r.

[45] A better estimate of the discharge of the whole, very large Amazon basin is obtained by dividing it into smaller SBs that have smaller lag times and comparing the estimates to the observed discharge time series (hydrograph). The surface inundation data set is then used in each SB to compute the lag time between estimated runoff and the time series of the inundation percentage at the location of the gauge by a simple lag correlation. Then the lagged discharge

Table 2. Relative, Bias, and RMS Error of Estimated Runoff From Different Data Combinations for the Whole Amazon SB

Data Combination	Relative (%)	Bias (mm/d)	RMSE (mm/d)
TMPA-PRI	48	−1.40	0.7
PERSIANN-PRI	60	−0.49	2.1
GPCP-PRI	31	−0.89	0.7
CMORPH-PRI	41	−1.18	1.2
TMPA-MON	23	−0.65	0.6
PERSIANN-MON	63	0.27	2.2
GPCP-MON	15	−0.43	0.60
CMORPH-MON	30	−0.40	1.1

is compared to the gauge observations for each SB. The computed lag–time for the smaller upstream SBs, 1, 3, 4, and 6, is zero months, while for the SBs 2, 5, 7, 8 and 11–14, it is one month. The lag-time for SBs 9 and 10 is also less than a month. Therefore accumulated delay time for the water from SBs 3 and 4 to reach mouth of the SB 12 is three months. The summed and lagged estimated total runoff will be explained more in Section 4.

[46] The relative uncertainty in a monthly estimates of R, $\upsilon\overline{R}$, can be estimated as the root mean square of the errors of each component divided by the value of R, assuming that the errors of the separate components are independent.

$$\upsilon_{\overline{R}} = \frac{\sqrt{\upsilon_{\overline{P}}^2\overline{P}^2 + \upsilon_{\overline{ET}}^2\overline{ET}^2 + \upsilon_{\overline{\Delta S}}^2\overline{\Delta S}^2}}{\overline{P} - \overline{ET} - \overline{\Delta S}} \tag{2}$$

[47] Given $\upsilon\overline{R}$, the relative error for $\overline{R}$, the 95% confidence limits on $\overline{R}$ are $\pm\upsilon_{\overline{R}}\overline{R}$. *Wahr et al.* [2004] estimated the GRACE uncertainties to about 1.0–1.5 cm for the Amazon basin. Therefore, the absolute error of the water storage changes between two observation months would be at least $\sqrt{2}$ times the of the one observation error (0.47–0.70 mm/d).

[48] The spatiotemporal variability of the absolute error for GPCP data is presented by *Huffman et al.* [2009]. The average error, $\upsilon_{\overline{P}}\overline{P}$, over the whole Amazon basin is 0.94 mm/d that ranges from 0.49 mm/d in SB 1 to 1.19 mm/d in SB 5. Note that the uncertainties for this product increases for the larger precipitation values. The uncertainties of other precipitation products are not available over South America at this time.

[49] Mean Absolute Error (MAE) of ET reported by *Mu et al.* [2007] is 0.33 mm/d in their improved version based on the evaluation at eddy flux towers. *Jimenez et al.* [2011] compared ET estimates of satellite based, re-analysis and other empirical methods globally and reported the largest absolute differences in monthly mean latent heat flux values over tropical regions; the maximum difference in Amazon SB is 24 W/m^2 (0.85 mm/d). Therefore, the assumption of ET uncertainty needs more evaluation. Note that the accuracy of the discharge measurements is not given from ORE-Hybam. However, analysis of the potential errors in river discharge measurements suggests that 5–10% is a reasonable estimation of the error in observed mean discharge [*Coe et al.*, 2002], which translates into 0.15–0.3 mm/day.

[50] The assumption of independent errors of each component needs a more careful investigation because derived ET estimates might depend on P estimates. In this step, only uncertainties of GPCP are available, and therefore will be used to compute the resultant uncertainties of the estimated runoff from equation (2) for this combination for all 14 SBs. Also note that the given equation (2) can only be used for the data with Gaussian distribution. Although P does not have Gaussian distribution, this formula can be used as a rough estimate about the uncertainty expecting even larger values dues to sever events.

4. Results

4.1. Estimates of Runoff and Choice of the Most Consistent Data Combination

[51] There are four P and three ET data sets available for this study, which produce different estimates of R (ΔS is taken only from GRACE). Table 2 shows the relative error, the total estimated error divided by the observed runoff values, Bias and RMSE of the estimated and observed runoff from different combinations of data over the whole Amazon. These error values are computed with different lag times: two months lag gives the maximum correlation (Min error) for most of the cases. Both TMPA and GPCP combined with ET-MON-M have smaller relative error compared to the observed value of 15 and 23%. Therefore ET-MON-M produces slightly smaller total error with two pairs of P than ET-PRI. On the other hand, PERSIANN based estimates produces larger error with both ET combinations and therefore is not used in the next.

[52] The estimated absolute error is 1 to 1.45 mm/d for the other three P pairs for the whole Amazon. To show more detail, the Bias and RMSE are computed at SB scale and shown in Table 3 for three P products. Since the annual variation of the TWS is small, we computed annual P-ET-R to obtain the bias and then removed it to compute the RMSE. This comparison shows where in the large Amazon basin, the estimated runoff works better and vice versa for each combination. The GPCP combination gives smaller RMSE in most of the SBs. In northern SBs 2–5 and SBs 11–12, RMSE shows large variation among three P combinations. Although the relative error shown in Table 2 is small (15% for GPCP, ET-MONM combination) for the whole Amazon, it is greater in smaller SBs especially in SBs 1,6,8 and 14 it increases as high as 128%.

[53] A dam controls the flow in SB 8 and therefore its storage changes differ from the natural rivers. This shows that one should be careful about using the smoother data because of loss of information that is a different effect than the attenuation effect investigated previously [*Chen et al.*, 2007]. While estimated runoff is in good agreement in amplitude and seasonal phase with observed runoff for all the SBs, except SB 3 (Figure 5), there is a phase lag and amplitude difference between the observed and estimated runoff for the entire Amazon basin, even for the combination with the best average agreement. This phase lag can arise because the satellite estimated runoff is averaged over the SB whereas the observed runoff represents integration at the mouth of the whole basin. Performing the same comparison in the smaller SBs supports this hypothesis: the results show much better agreement in phase and amplitude in all cases (Table 3). Mean absolute errors for each SB from both P-ET combinations are shown in Table 4 along with the estimated uncertainties. Comparison of the uncertainties and MAE (mean absolute error) in Table 4 shows that the errors are not always within the uncertainties for all of the

Table 3. Bias and RMSE of the Estimated Runoff From Different P, and ET Data in Different SBs of Amazon (mm/d)[a]

	GPCP, ET-MON-M		GPCP, ET-PRI		CMORPH, ET-MON-M		CMORPH, ET-PRI		TMPA, ET-MON-M		TMPA, ET-PRI	
SBs	Bias	RMSE	Bias	RMSE	Bias	RMSE	Bias	RMSE	Bias	RMSE	Bias	RMSE
1	−3.2	1.1	−4.0	1.1	−3.6	1.4	−4.4	1.4	−4.4	1.3	−5.2	1.3
2	−1.1	0.6	−1.3	0.8	−0.8	1.5	−1.0	1.5	−2.1	0.9	−2.3	1.1
3	−2.1	1.3	−2.9	1.5	−0.8	2.6	−1.6	2.6	−2.4	1.5	−3.2	1.7
4	0.0	1.1	−0.8	1.1	1.2	2.1	0.4	2.1	−0.4	1.8	−1.1	1.8
5	0.2	1.2	−0.9	1.2	1.9	2.2	0.8	2.3	−0.4	1.8	−1.5	1.7
6	0.9	0.9	−0.3	0.9	0.2	1.3	−1.0	1.2	−0.3	1.1	−1.4	1.0
7	−0.1	0.7	−0.7	1.0	1.2	1.7	0.6	1.8	−0.7	0.9	−1.3	1.0
8	−0.4	0.8	−0.5	0.8	0.4	1.2	0.3	1.2	−0.7	0.8	−0.7	0.8
9	−0.1	0.8	−0.3	0.8	0.6	1.1	0.4	1.2	−0.7	0.8	−0.9	1.0
10	−0.5	1.1	−1.1	1.2	1.3	1.2	0.8	1.5	−0.7	1.3	−1.3	1.4
11	−1.2	1.4	−2.2	1.4	1.2	2.5	0.2	2.5	−1.7	1.5	−2.6	1.5
12	0.3	1.4	−0.8	1.5	1.4	1.9	0.3	2.0	0.2	1.3	−1.0	1.5
13	−0.3	0.6	−1.1	0.7	1.4	1.0	0.5	1.0	−0.2	0.6	−1.0	0.7
14	0.7	0.8	−0.2	0.9	2.3	1.4	1.4	1.3	0.5	0.8	−0.4	0.9

[a]Bias is computed as a difference of annual P-ET-R.

SBs; but are very close to these values except for the large differences in SB 1 and 3. This could be due to major limitations of satellite data sets over mountainous regions, highlighted in [*Sorooshian et al.*, 2011] but also is seen in other in situ based studies below.

[54] *Coe et al.* [2002] used the IBIS ecosystem model, together with the HYDRA surface hydrology model, to simulate the Amazon Basin flooded area and discharge from historical climate records from 1939 to 1998. Evaluation of their results against diverse observations indicates that estimates of precipitation are likely greatly underestimated outside of the Brazilian portion of the Amazon Basin. As a result, flooded area and discharge and are consistently underestimated for watersheds with significant input from non-Brazilian portions of the basin [*Coe et al.*, 2002]. *Costa and Foley* [1997] found a similar negative bias in their simulated discharge of the Andes SBs and concluded that estimations of the runoff for Andes SBs were unusually low compared to those inside Brazil and suggested that this large negative bias is likely associated with errors in the precipitation data set outside Brazil rather than with the calculation of evapotranspiration. Also some other studies of rainfall variability in the Amazon basin using a large number of rainfall gauges showed that rainfall decreases at higher altitudes in the Andes [*Espinoza Villar et al.*, 2009a, 2009b]. GPCP V2.1 and TRMM3B42 data are adjusted to monthly gauge data (but different versions), but this adjustment does not increase significantly the microwave-based estimates in SB 1. Although GPCP version 2.1 has larger rainfall estimates in the Andes than the previous version [*Huffman et al.*, 2009], there is still a large difference between incoming and outgoing components of the water balance. Even CMORPH and PERSIANN data, which rely solely on satellite measurements and over-estimate rainfall in other parts of the Amazon, give smaller estimates than GPCP in the Andes.

[55] To evaluate the evapotranspiration data, we note that the net radiation used to produce the ET-PRI is generally larger over rain forest areas than that used to produce other remote sensing-based ET data sets [*Jimenez et al.*, 2011]. Since radiation is the most important term in the Penman-Monteith formula, this difference can explain the larger ET values obtained for the Amazon. As seen in Table 3, after removing bias from the estimates, RMSE values are generally smaller in ET-MON-M based combinations except in SBs 4, 5, 6, 8 and 11 where it is the same for both ET estimates. ET-MON-M is chosen for further study of the dynamics since there is no objective basis for removing the bias from ET-PRI.

4.2. Estimated Runoff Using Lagging Method

[56] As mentioned in the comparison of the estimated and observed seasonal variations of runoff, there are magnitude differences and a phase lag between the two estimates for the whole Amazon basin (at the downstream station) but not in the smaller SBs. Therefore, the method used in the smaller SBs to shift the observed runoff is applied at this stage to estimate the total runoff at the mouth of the whole Amazon similar to an element-to-element routing method. The estimated runoff downstream is the sum of the runoff from each upstream SB with a lag time computed from the lag correlation analysis between inundation data and estimated runoff. These correlation computations are used to determine the accumulated flow into SBs 10 and 3, then into SB 11 and finally into SB 12. The lag times from each

Table 4. Mean Absolute Error of the Estimated Runoff From Two Different P and ET Combinations and Estimated Uncertainty of the GPCP and ET-MON-M Data for Different SBs

	GPCP, ET-MON-M		CMORPH, ET-PRI
SB	Estimated Total Uncertainties (mm/d)	Mean Absolute Error (mm/d)	Mean Absolute Error (mm/d)
1	0.78	3.03	4.12
2	1.11	1.00	2.14
3	1.26	2.14	3.98
4	1.31	1.38	2.79
5	1.34	1.27	2.89
6	1.07	1.37	2.27
7	1.16	1.33	2.36
8	0.95	0.90	1.13
9	1.03	0.86	1.24
10	1.12	1.28	2.20
11	1.23	1.74	2.83
12	1.17	1.63	2.25
13	1.15	1.03	1.57
14	1.12	1.69	2.18
Whole	1.03	1.37	1.75

Table 5. Distance and Travel Time From Mouth of Each SB to the Obidos Station Along With the Total Lag Time From the Upstream of Each SB to Its Mouth

SB	Distance (km Mouth-to-Mouth)	Travel Time Range (v = 0.45–0.9 m/s) days	Total Lag Time (months)
1	3300	43–86	3
2	2200	29–58	3[a]
3	1800	24–48	2
4	1650	22–44	1
5	1350	17–35	1
6	1400	18–36	1
7	1800	23–47	2
8	1850	24–48	1
9	1450	18–38	1
10	780	10–20	0
11	750	10–20	1
12	0	0	0
13	0	0	1[a]
14	0	0	1[a]

[a]The total lag time has one month inter-SB travel time.

source are computed as the flow length divided by the velocity of the flow. As a first estimate of the average velocity, we use 1.5 miles/hr according to Smithsonian National Zoological Park. Then the time series of the lagged estimated runoff for different SBs is compared to the time series of inundation to adjust the velocity. Table 5 shows the lag time based on the assumed velocity range from the mouth of each upstream SB to the mouth of the SB 12 (Obidos station) and the best-correlated lag-time with the inundation data set. The total lag-time indicates the average travel time needed from the mouth of the SB to mouth of the whole Amazon plus the intraSB travel time. This intraSB time varies for different SBs depending on the shape and size of the SB. SBs with one-month intraSB lag time are marked with an asterisk. The total travel time for the flow from SBs 1 and 2 to downstream is three months.

[57] The correlation coefficient between lagged estimated runoff and observed increases from 0.72 to 0.88 using the GPCP and ET-MON-M combination and from 0.68 to 0.90 using the TMPA and ET-MON-M combination. Similarly, the RMSE decreases from 0.98 to 0.61 for GPCP and from 0.95 to 0.84 for TMPA. The estimated runoff from this method, for the whole Amazon is compared in Figure 7 to the observed runoff and the previous (unadjusted) values. Figure 7 shows that the lagged runoff at the mouth of the whole Amazon agrees much better in phase and magnitude with the observed data which supports our explanation and does not require including underground discharge to resolve the differences as described by *Syed et al.* [2005].

[58] Using GPCP data for precipitation, ET-MON-M for evapotranspiration, GRACE with smoothing radius of 500km for total water storage changes and the observed discharge data, the imbalance, relative error in the basin is decreased compared with previous studies from 50% [*Marengo*, 2005] to 21% over the whole basin. Generally, estimated runoff using the GPCP-MON combination is higher than observed in the northern parts of the Amazon basin but significantly lower in the western parts, mostly because of uncertainties in the precipitation data. Dividing the basin into five parts with similar climate and SB response, the total absolute error in the western parts of Amazon is 0.3 mm/d (SB 1, 2, 3), 0.17 mm/d in the northern part (SBs 4, 5, 6), 0.23 mm/d in the southern Amazon (7, 8, 9), 0.25 mm/d in central downstream (SBs 11 and 12), and

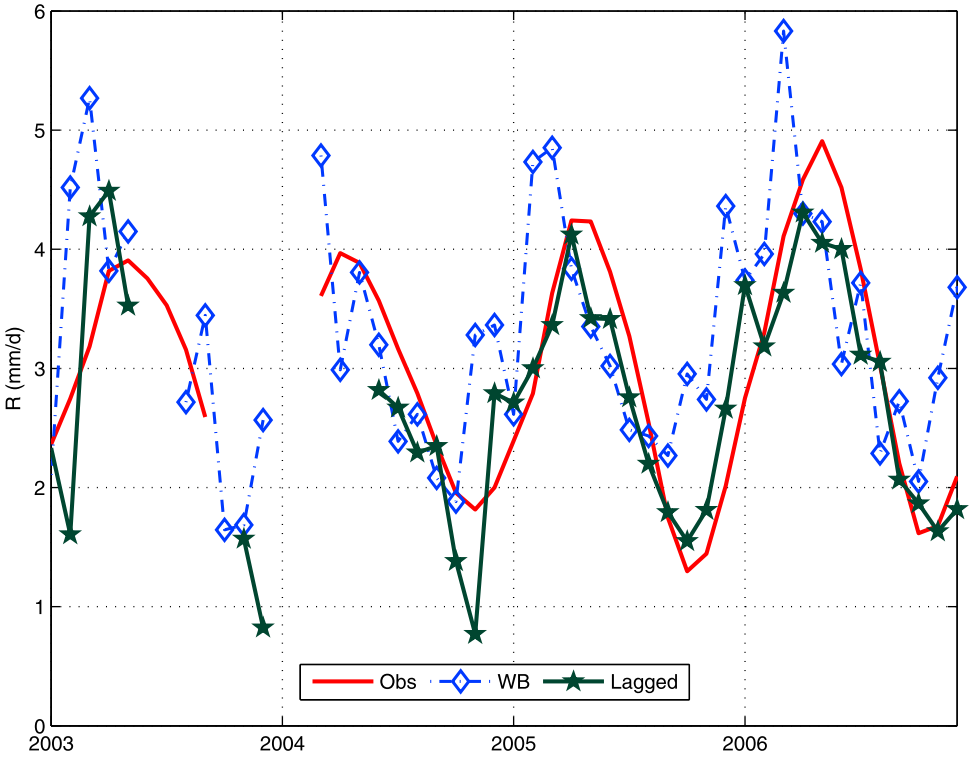

Figure 7. Comparison of observed total runoff with estimated runoff from WB and after lagging method using GPCP combination for 2003–2006. Total error decreased from 1.1 mm/d to 0.65 mm/d (21%).

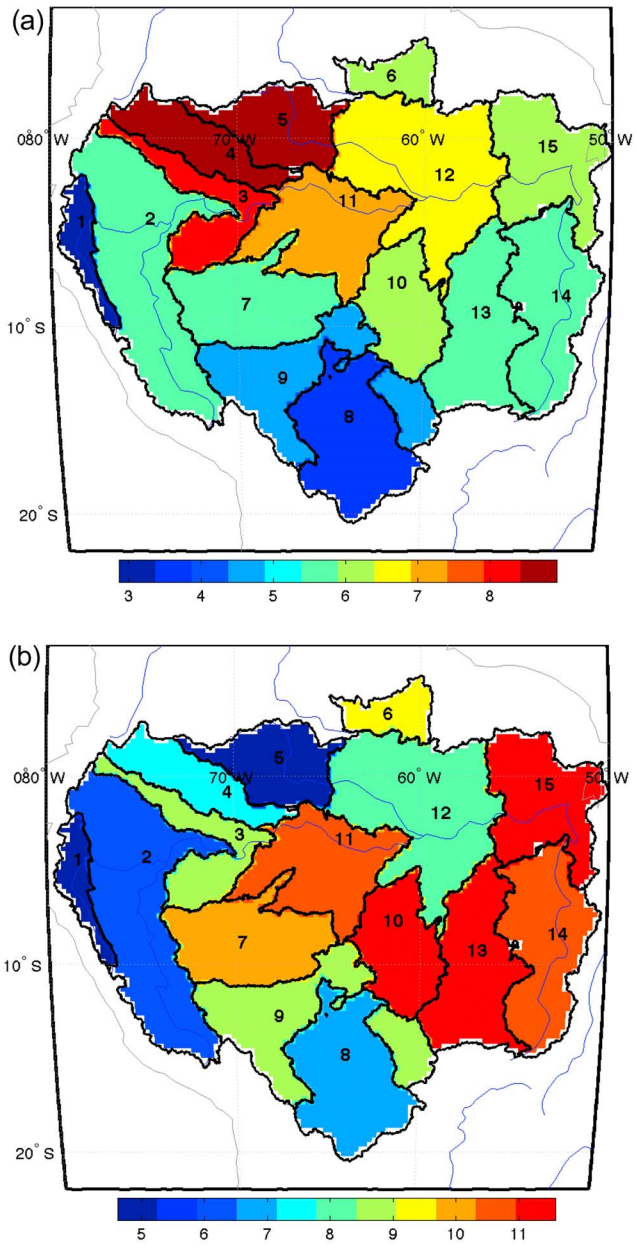

Figure 8. (a) Annual precipitation and (b) its seasonal range (max-min) (mm/d) in different SBs using GPCP for different SBs for 2003–2006. For more information on SBs see Table 1.

0.22 mm/d in the eastern Amazon (SB 10, 13, 14) relative to the area of the whole Amazon basin (total error multiplied by relative area of the section of Amazon). The average precipitation, evaporation and runoff over the 14 SBs of Amazon are thus 6.33, 3.27 and 3.07 mm/d, respectively.

4.3. Spatiotemporal Variation of the Water Budget Components Using the Most Consistent Data Combination

[59] Figure 8 shows the mean and seasonal variation, as a difference of extreme values, of the precipitation estimates from GPCP data. While the northwestern sub-basins receive the largest rainfall amounts, they exhibit smaller seasonal variations such that they never have a dry season with rainfall less than 3.3 mm/d. The eastern SBs, 10, 13, 14, and 15 have larger seasonal variations of 10–12 mm/d despite generally smaller annual mean amounts. Generally the western SBs have the wet season prior to the eastern SBs. Note also that precipitation in SB 6 has the opposite seasonal variation than the other SBs because of its latitudes.

[60] The mean ET map from ET-MON-M in Figure 9a shows values from about 3 to 3.6 mm/d over the Amazon, smaller in SBs 6, 8 and 9 with partly flooded Savannah vegetation and SB 2 located in the Andes. Seasonal variability of ET (Figure 9b) varies among the SBs, exhibiting maximum variation in SBs (5, 8, 12, 15). Maximum ET

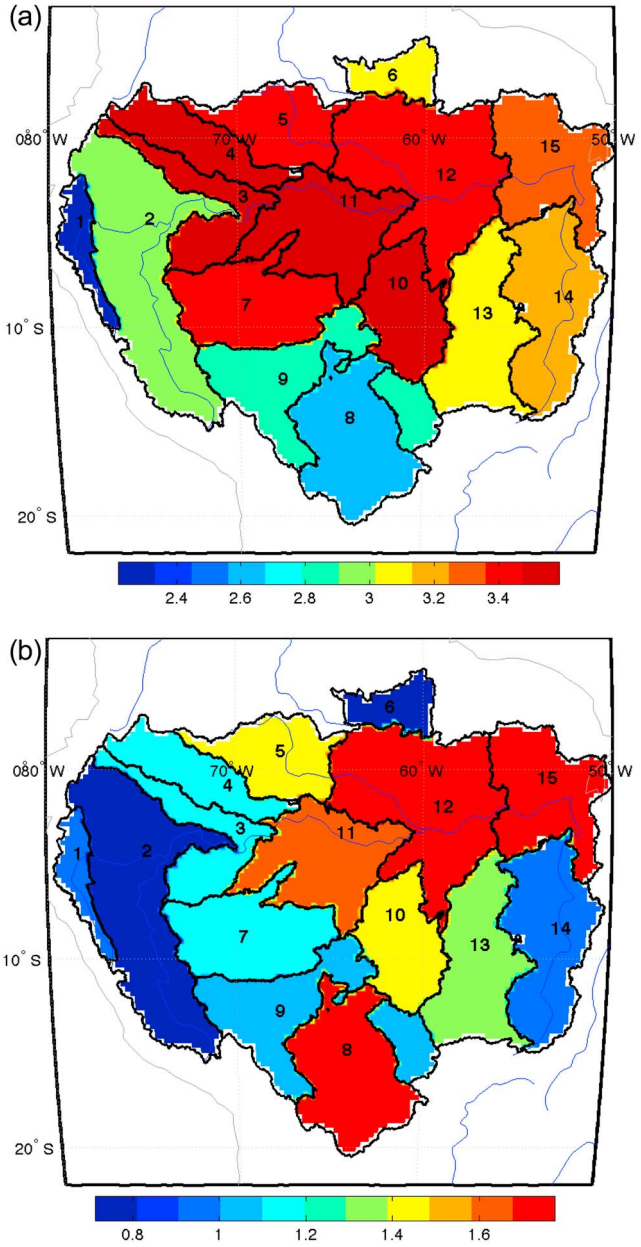

Figure 9. (a) Mean annual evapotranspiration and (b) its seasonal range (max-min) (mm/d) for different SBs (numbers) using ET-MON for 2003–2006. For more information on SBs see Table 1.

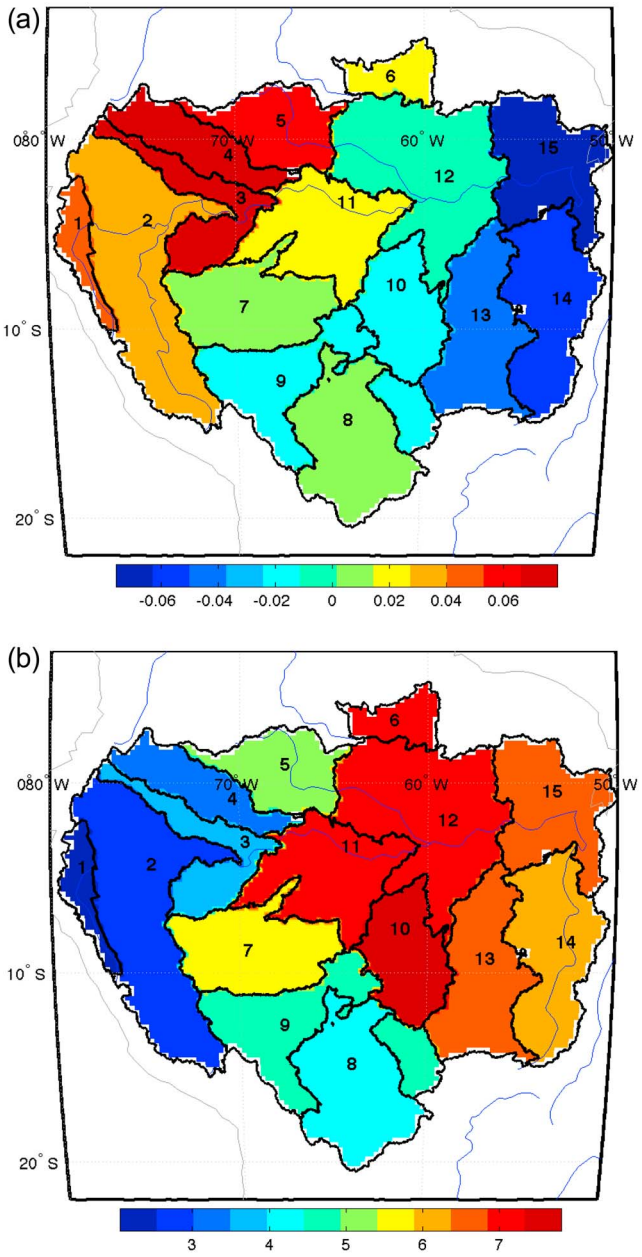

Figure 10. (a) Mean and annual water storage changes and (b) their seasonal range (max-min) (mm/d) using GRACE 500km smoothing radius for 2003–2006. For more information on SBs see Table 1.

accruing in the dry season in these particular forested SBs (11, 12, 15) from all three ET estimates is consistent with the analysis by *Betts and Silva Dias* [2010] and *da Rocha et al.* [2004, 2009], which they explain by larger radiation in this season and more water storage (drainage from upstream SBs). However, SB 8 has larger ET in the wet season because of the water stress in a longer dry season (Figure 3). The vegetation type of this SB is savannah, which makes it different than SB 11 and 12.

[61] The annual mean and variance of the total water storage (TWS) are shown in Figure 10 from the JPL 500 km smoothing radius version. The annual mean is negligible for the most of the SBs (±0.07 mm/d) with a positive sign in the western SBs and a negative sign in the eastern ones. Seasonal variation of TWS (Figure 10b), as a difference of maximum and minimum, shows SBs with larger storage variation due to accumulation of water from upstream SBs. In Figure 10, SB 15 which is outlet of the whole Amazon, shows smaller seasonal variation that the upstream SBs although its intrabasin P and ET have large variations. This is because this SB and SB12 receive contributions from upstream SBs with different wet and dry seasons and therefore are flooded during their local dry seasons.

[62] Annual mean and seasonal variation of discharge are shown in Figure 11 based on In situ data. Northwestern SBs shows larger contributions in net runoff than southern SBs;

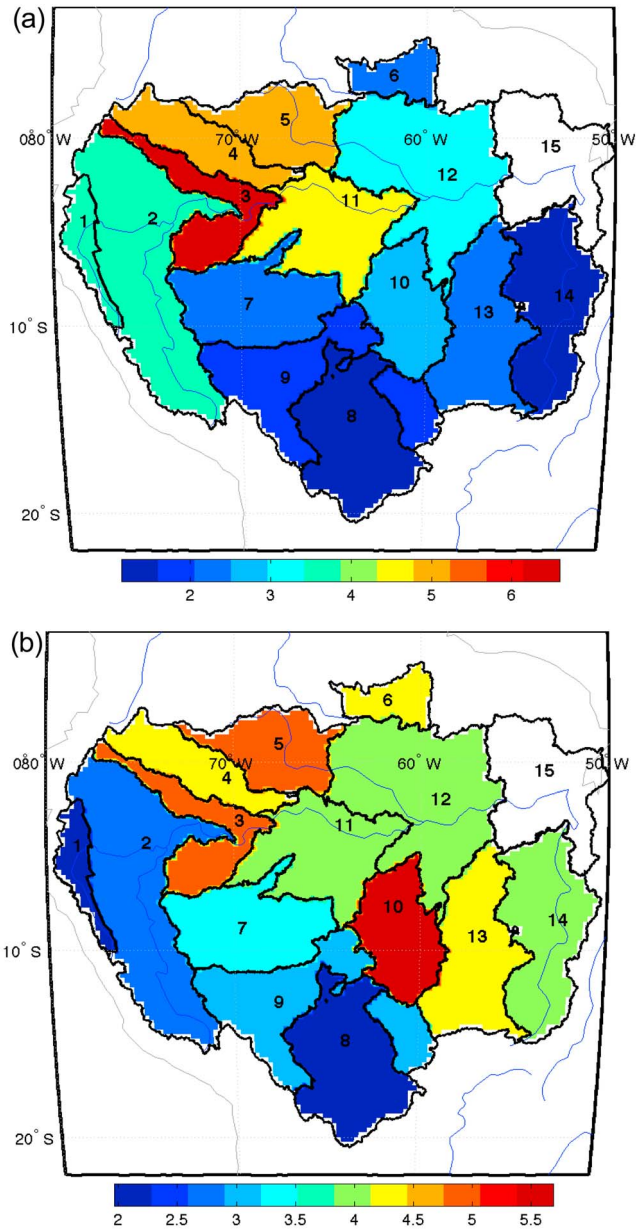

Figure 11. (a) Mean and (b) seasonal range (max-min) of runoff (mm/d) for different SBs using in situ data for 2003–2006. For more information on SBs see Table 1.

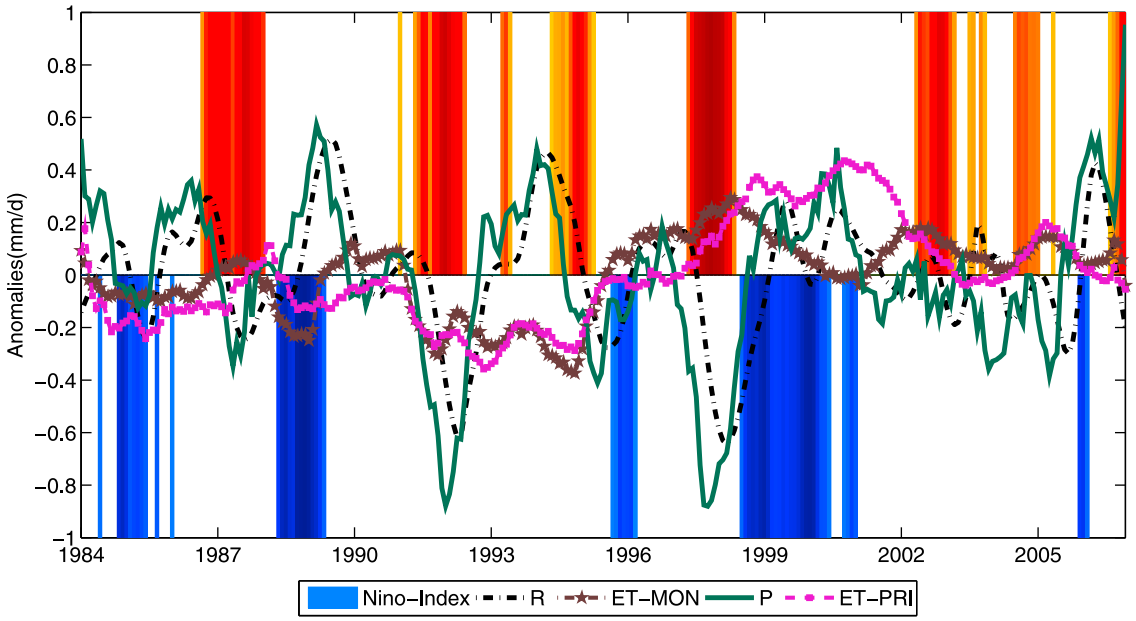

Figure 12. Normalized de-seasonalized anomalies of water budget components for the entire Amazon basin. P based on GPCP, ET from ET-PRI and ET-Mon-Z, R is in situ measurements. Indexed Large ENSO events with positive and negative signs are shaded.

but the larger areas of the latter ones produce large discharge to the outlet of Amazon. The distribution of annual net runoff among the SBs follows the precipitation distribution: the largest discharge is observed in northwest SBs (3 to 5) with the largest annual mean precipitation. In particular, SB 3 exhibits maximum monthly discharge up to 12 mm/d because of its large P rates and also smaller storage variations. Since this component is response of the variations of other components of the water budget, its seasonal variation follows the combination of other three (Figures 8b, 9b, 10b and 11b).

5. Dynamics of the Water Budget

[63] After choosing the most consistent data set for precipitation and evapotranspiration, along with inundation data and observed runoff and storage changes, we investigate the dynamics of the water balance in the Amazon SBs. Since the whole Amazon has a very large drainage area within which wet and dry seasons, vegetation and topography all vary, study of the dynamics provides more detail on the interaction of the atmosphere and land and might provide a clearer indication of the controlling processes. The temporal variations of each component of the water budget are displayed in Figures 8, 9, 10 and 11 and discussed in Section 4.

[64] These components are linked temporally so that generally when rainfall increases in the wet season, ET, R and TWS change as a response. Usually this response is an increase but there are some contradictory cases that will be discussed here. For instance, TWS in SB 12 is a minimum during the dry season and decreased runoff in upstream SBs while its local dry season occurs two months later (Figure 4). ET in SBs 5, 11, 12, and 15 with short dry seasons increases with decreasing P in the dry season because of increased net radiation (Figure 3). This increase of ET in the dry season in the eastern tropical forests is reported in extended measurements during LBA by *da Rocha et al.* [2004] and *Goulden et al.* [2004] and contradicts earlier studies showing little seasonal variation of ET. Conversely, reanalysis ET data from ERA-40, exhibits larger seasonal variations of ET because of insufficient moisture storage in the model root-zone [*Betts and Silva Dias*, 2010].

[65] To investigate inter-annual variation of the water budget components, normalized and de-seasonalized anomalies of each component are computed for the entire Amazon basin and displayed in Figure 12 for the 1984–2006 period. Note that since TWS from GRACE is available after 2002, it is not included in this analysis and therefore observed runoff is used. Generally there are opposite sign anomalies of P and ET while runoff anomalies follow P with a lag. Although the total anomalies are not sensitive to El Niño-Southern Oscillation (ENSO) indices (correlation coefficients less that 0.5), in extreme events they exhibit larger variation. The two ET estimates have a better agreement in interannual variability except during La-Nina of 1999 when ET-PRI increases with the increased P while ET-Zhang decreases.

[66] Figure 13 shows the standard deviation of de-seasonalized anomalies of the three components (P, ET and R) based on GPCP, ET-Zhang and in situ runoff gauges. Northern and downstream eastern SBS exhibit large interannual variability. These anomalies are as large as 0.82 mm/d for P, 0.22 for ET and 0.80 mm/d for R. Since these SBs also show large annual mean values, these results are expected. This might also suggest that in order to investigate long-term and significant variability of the water in Amazon, one should focus on these regions.

[67] In order to analyze the impact of ENSO events on the water budget components of Amazon SBs, they are divided into their local wet and dry seasons because of the seasonal impact of these events. Out of 15 SBs of the Amazon, only

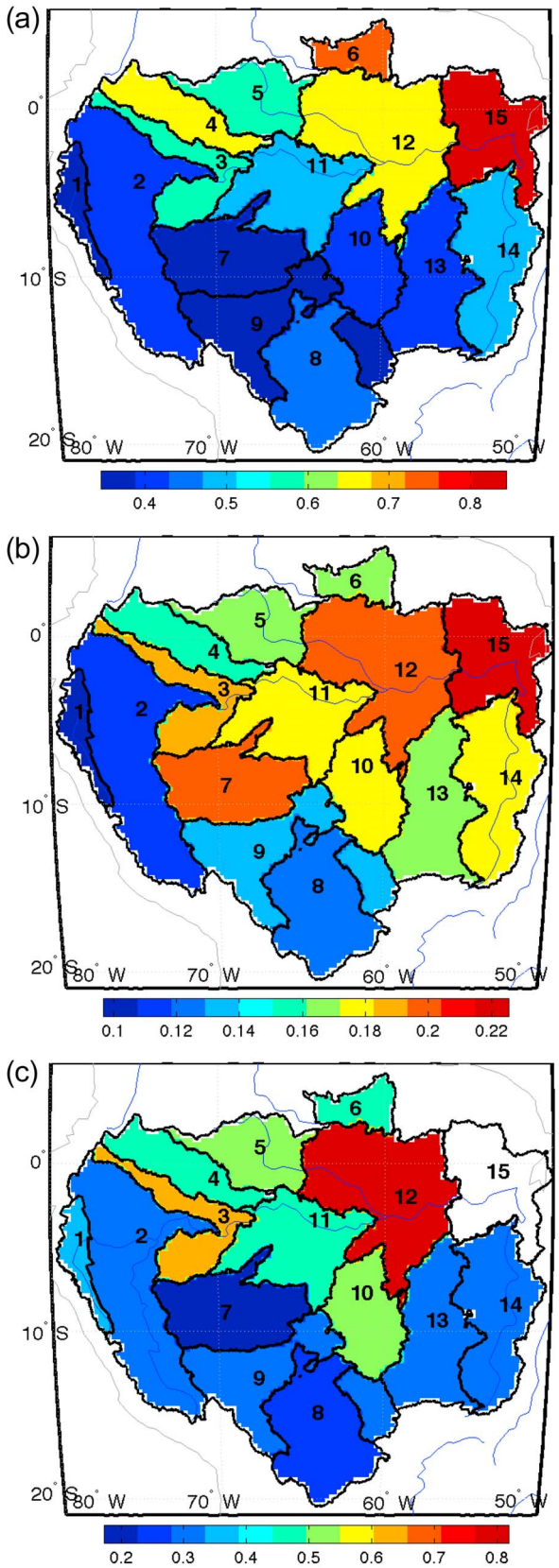

Figure 13. Interannual standard deviation (mm/d) of (a) P based on GPCP, (b) ET based on ET-Zhang, and (c) R based on gauges from 1984 to 2006 after filtering high frequencies using 12 months running mean.

four exhibit significant correlation to ENSO. Precipitation in SBs 5, 6, and 12 show significant correlations of 0.65 to 0.8 with the Pacific Nino index (Nino 3.4) for the Dec-Feb months. Runoff follows P with a lag time in SBs 5, 6, and 11 and also is cross-correlated in SB 12 to ENSO (−0.65) during its dry season. ET does not show any significant correlation with the ENSO for the entire Amazon.

6. Summary and Conclusions

[68] This study focuses on the spatial and seasonal variability of the water budget components of the Amazon using different combination of remote sensing data products and observed gauge measurements. New information about TWS changes from GRACE and satellite based ET estimates are used to evaluate terrestrial water balance for more than four years at intrabasin and whole basin scales. Different data sets for precipitation and evaporation are examined and the most consistent data combination is selected for the study of dynamics using a land water balance approach and spatiotemporal consistency. The best data set for precipitation is GPCP in combination with ET data from University of Montana. The average annual rainfall for the entire basin from GPCP is 6.33 mm/d, evaporation from ET-MON-M is 3.28 and runoff from in situ data is 3.06 mm/d. This method based on water balance give smaller RMSE than previous atmospheric moisture convergence method [*Syed et al.*, 2005] (0.61 and 1.28 mm/d respectively) over the Amazon basin and has a potential to be used to estimate discharge at different sub-parts of a large tropical basin.

[69] Study of intrabasin dynamics, based on the consistent data set, shows that the water budget components, except ET, exhibit large seasonal variations within the Amazon basin. The northwest SBs have the largest rainfall amounts, approximately 8.5 mm/d, while the southern SBs average 5 mm/d. Storage change is also very dynamic and is larger during the extreme changes of the intraSB precipitation. For the two downstream SBs the seasonal variation is stronger during the dry and wet seasons of their upstream SBs with larger discharge contribution.

[70] The estimated runoff time series have better agreement at SB scale than the total runoff for the whole Amazon. Therefore the estimated runoff from the balance method for each SB is integrated downstream using an element-to-element routing method. An inundation data set is used to compute delay times instead of specifying flow velocities. This delay time is computed based on the maximum lag-correlation between upstream and downstream SBs. The estimated lagged runoff resolves the dynamics of the surface runoff better and can be used to estimate the runoff in different parts of the large Amazon. The absolute monthly error for the whole Amazon basin decreases from 1.1 to 0.61 mm/d for the GPCP and ET-MON-M combination using the lagging method. This lagging method based on the TWS from GRACE and time series of inundation fractions is simple since it does not need assumptions about the channel Manning roughness and slope of the river and therefore, can be used in distributed routing models to get the hydrograph (time series) of the runoff at different locations for any large-scale watershed.

[71] Interannual variation of the de-seasonalized anomalies of P, ET, R for a longer period of 23 years are inves-

tigated for the whole basin. During this period, there are large anomalies in all of these three components especially during ENSO events. The spatial pattern of the interannual variation of the components follows the mean annual values so that these anomalies are smaller in southern SBs and larger in northern and downstream SBs.

[72] There are diverse uncertainties among different remote sensing retrieved data that affect water balance in the basin. The estimated uncertainty for GPCP is 0.9 mm/d over the entire basin [*Huffman et al.*, 2009], but larger biases occur in the smaller SBs 1 and 3 located in Andes and northwest part of the Amazon, exhibiting underestimates of 3.2 and 2.3 mm/d, respectively, based on water balance. Comparison of two different ET estimates shows that there is 1 mm/d difference between them over the Amazon. Seasonality is not significant in evaporation except for southern SB 8 with Savannah vegetation and in Negro and Amazon rivers as large as 0.6 mm/d as a result of water stress at SB 8 during the dry season and decreased cloudy days and larger net radiation in latter (SBs 5, 11 and 12). This is seen in all three remote sensing based ET data sets while earlier reanalysis-based ET estimates did not show this pattern. Also the effect of smoothing the GRACE data can introduce more uncertainties to the data.

[73] Improvements in remote sensing products especially time resolution, may come from the future GPM for precipitation, soil moisture from SMOS and SMAP, and runoff from the SWOT mission and may help reduce the uncertainties in the water budget and increase the knowledge of dynamics at finer time scales over the tropics. Also, other procedures for analyzing GRACE data might help to reduce noise and attenuation effects of smoothing of the data sets.

[74] **Acknowledgments.** NASA Energy and Water cycle Study, grant NNXD7AO90G and NOAA-CREST, grant NA06OAR4810162, funding supported this research. The authors would like to thank Q. Mu, K. Zhang and J. Sheffield for sharing their evapotranspiration data sets and the science teams of the GPCP, CMORPH, PERSIANN and TRMM and GRACE for providing public data source.

References

Adler, R. F., et al. (2003), The version-2 global precipitation climatology project (GPCP) monthly precipitation analysis (1979-present), *J. Hydrometeorol.*, *4*(6), 1147–1167, doi:10.1175/1525-7541(2003)004<1147:TVGPCP>2.0.CO;2.

AghaKouchak, A., A. Behrangi, S. Sorooshian, K. Hsu, and E. Amitai (2011a), Evaluation of satellite-retrieved extreme precipitation rates across the central United States, *J. Geophys. Res.*, *116*, D02115, doi:10.1029/2010JD014741.

AghaKouchak, A., N. Nasrollahi, J. J. Li, B. Imam, and S. Sorooshian (2011b), Geometrical Characterization of precipitation patterns, *J. Hydrometeorol.*, *12*(2), 274–285, doi:10.1175/2010JHM1298.1.

Alsdorf, D. E. (2003), Water storage of the central Amazon floodplain measured with GIS and remote sensing imagery, *Ann. Assoc. Am. Geogr.*, *93*(1), 55–66, doi:10.1111/1467-8306.93105.

Alsdorf, D. E., and D. P. Lettenmaier (2003), Tracking fresh water from space, *Science*, *301*(5639), 1491–1494, doi:10.1126/science.1089802.

Alsdorf, D., P. Bates, J. Melack, M. Wilson, and T. Dunne (2007), Spatial and temporal complexity of the Amazon flood measured from space, *Geophys. Res. Lett.*, *34*, L08402, doi:10.1029/2007GL029447.

Betts, A. K., and M. A. F. Silva Dias (2010), Progress in understanding land-surface-atmosphere coupling from LBA research, *J. Adv. Model. Earth Syst.*, *2*, 6, doi:10.3894/JAMES.2010.2.6.

Bjerklie, D. M., S. L. Dingman, C. J. Vorosmarty, C. H. Bolster, and R. G. Congalton (2003), Evaluating the potential for measuring river discharge from space, *J. Hydrol.*, *278*(1–4), 17–38, doi:10.1016/S0022-1694(03)00129-X.

Bullock, A., and M. Acreman (2003), The role of wetlands in the hydrological cycle, *Hydrol. Earth Syst. Sci.*, *7*(3), 358–389, doi:10.5194/hess-7-358-2003.

Chen, J., C. Wilson, J. Famiglietti, and M. Rodell (2007), Attenuation effect on seasonal basin-scale water storage changes from GRACE time-variable gravity, *J. Geod.*, *81*(4), 237–245, doi:10.1007/s00190-006-0104-2.

Chen, J. L., C. R. Wilson, and B. D. Tapley (2010), The 2009 exceptional Amazon flood and interannual terrestrial water storage change observed by GRACE, *Water Resour. Res.*, *46*, W12526, doi:10.1029/2010WR009383.

Coe, M. T., M. H. Costa, A. Botta, and C. Birkett (2002), Long-term simulations of discharge and floods in the Amazon Basin, *J. Geophys. Res.*, *107*(D20), 8044, doi:10.1029/2001JD000740.

Costa, M. H., and J. A. Foley (1997), Water balance of the Amazon Basin: Dependence on vegetation cover and canopy conductance, *J. Geophys. Res.*, *102*(D20), 23,973–23,989, doi:10.1029/97JD01865.

Dai, A., and K. E. Trenberth (2002), Estimates of freshwater discharge from continents: Latitudinal and seasonal variations, *J. Hydrometeorol.*, *3*(6), 660–687, doi:10.1175/1525-7541(2002)003<0660:EOFDFC>2.0.CO;2.

da Rocha, H. R., M. L. Goulden, S. D. Miller, M. C. Menton, L. Pinto, H. C. de Freitas, and A. Figueira (2004), Seasonality of water and heat fluxes over a tropical forest in eastern Amazonia, *Ecol. Appl.*, *14*(sp4), 22–32, doi:10.1890/02-6001.

da Rocha, H. R., et al. (2009), Patterns of water and heat flux across a biome gradient from tropical forest to savanna in Brazil, *J. Geophys. Res.*, *114*, G00B12, doi:10.1029/2007JG000640.

Decharme, B., H. Douville, C. Prigent, F. Papa, and F. Aires (2008), A new river flooding scheme for global climate applications: Off-line evaluation over South America, *J. Geophys. Res.*, *113*, D11110, doi:10.1029/2007JD009376.

Espinoza Villar, J. C. E., J. L. Guyot, J. Ronchail, G. Cochonneau, N. Filizola, P. Fraizy, D. Labat, E. de Oliveira, J. J. Ordonez, and P. Vauchel (2009a), Contrasting regional discharge evolutions in the Amazon basin (1974–2004), *J. Hydrol. Amsterdam*, *375*(3–4), 297–311, doi:10.1016/j.jhydrol.2009.03.004.

Espinoza Villar, J. C., J. Ronchail, J. L. Guyot, G. Cochonneau, F. Naziano, W. Lavado, E. De Oliveira, R. Pombosa, and P. Vauchel (2009b), Spatio-temporal rainfall variability in the Amazon basin countries (Brazil, Peru, Bolivia, Colombia, and Ecuador), *Int. J. Climatol.*, *29*(11), 1574–1594, doi:10.1002/joc.1791.

Fekete, B. M., C. J. Vörösmarty, and W. Grabs (2002), High-resolution fields of global runoff combining observed river discharge and simulated water balances, *Global Biogeochem. Cycles*, *16*(3), 1042, doi:10.1029/1999GB001254.

Fisher, J. B., K. P. Tu, and D. D. Baldocchi (2008), Global estimates of the land-atmosphere water flux based on monthly AVHRR and ISLSCP-II data, validated at 16 FLUXNET sites, *Remote Sens. Environ.*, *112*(3), 901–919, doi:10.1016/j.rse.2007.06.025.

Frappart, F., F. Papa, J. S. Famiglietti, C. Prigent, W. B. Rossow, and F. Seyler (2008), Interannual variations of river water storage from a multiple satellite approach: A case study for the Rio Negro River basin, *J. Geophys. Res.*, *113*, D21104, doi:10.1029/2007JD009438.

Frappart, F., F. Papa, A. Guntner, S. Werth, G. Ramillien, C. Prigent, W. B. Rossow, and M. P. Bonnet (2010), Interannual variations of the terrestrial water storage in the Lower Ob' Basin from a multisatellite approach, *Hydrol. Earth Syst. Sci.*, *14*(12), 2443–2453, doi:10.5194/hess-14-2443-2010.

Getirana, A. C. V., M.-P. Bonnet, O. C. Rotunno Filho, W. Collischonn, J.-L. Guyot, F. Seyler, and W. J. Mansur (2010), Hydrological modelling and water balance of the Negro river basin: Evaluation based on in situ and spatial altimetry data, *Hydrol. Processes*, *24*, 3219–3236, doi:10.1002/hyp.7747.

Gibson, J. K., P. Kållberg, S. Uppala, A. Nomura, A. Hernandez, and E. Serrano (1997), ERA description, *Re-Analysis Final Rep. Ser. 1*, 71 pp., ECMWF, Reading, U. K.

Goulden, M. L., S. D. Miller, H. R. da Rocha, M. C. Menton, H. C. de Freitas, A. Figueira, and C. A. D. de Sousa (2004), Diel and seasonal patterns of tropical forest CO2 exchange, *Ecol. Appl.*, *14*(sp4), 42–54, doi:10.1890/02-6008.

Gu, G. J., R. F. Adler, G. J. Huffman, and S. Curtis (2007), Tropical rainfall variability on interannual-to-interdecadal and longer time scales derived from the GPCP monthly product, *J. Clim.*, *20*(15), 4033–4046, doi:10.1175/JCLI4227.1.

Hsu, K., X. Gao, S. Sorooshian, and H. V. Gupta (1997), Precipitation estimation from remotely sensed information using artificial neural networks, *J. Appl. Meteorol.*, *36*, 1176–1190, doi:10.1175/1520-0450(1997)036<1176:PEFRSI>2.0.CO;2.

Huffman, G. J., R. F. Adler, D. T. Bolvin, G. J. Gu, E. J. Nelkin, K. P. Bowman, Y. Hong, E. F. Stocker, and D. B. Wolff (2007), The TRMM multisatellite precipitation analysis (TMPA): Quasi-global, multiyear, combined-sensor precipitation estimates at fine scales, *J. Hydrometeorol.*, *8*(1), 38–55, doi:10.1175/JHM560.1.

Huffman, G. J., R. F. Adler, D. T. Bolvin, and G. J. Gu (2009), Improving the global precipitation record: GPCP Version 2.1, *Geophys. Res. Lett.*, *36*, L17808, doi:10.1029/2009GL040000.

Jimenez, C., et al. (2011), Global intercomparison of 12 land surface heat flux estimates, *J. Geophys. Res.*, *116*, D02102, doi:10.1029/2010JD014545.

Joyce, R. J., J. E. Janowiak, P. A. Arkin, and P. P. Xie (2004), CMORPH: A method that produces global precipitation estimates from passive microwave and infrared data at high spatial and temporal resolution, *J. Hydrometeorol.*, *5*(3), 487–503, doi:10.1175/1525-7541(2004)005<0487:CAMTPG>2.0.CO;2.

Kanamitsu, M., W. Ebisuzaki, J. Woollen, S. K. Yang, J. J. Hnilo, M. Fiorino, and G. L. Potter (2002), NCEP-DOE AMIP-II reanalysis (R-2), *Bull. Am. Meteorol. Soc.*, *83*(11), 1631–1643, doi:10.1175/BAMS-83-11-1631.

Leopoldo, P. R., W. Franken, E. Salati, and M. N. Ribeiro (1987), Towards a water-balance in the central Amazonian region, *Cell. Mol. Life Sci.*, *43*(3), 222–233, doi:10.1007/BF01945545.

Marengo, J. A. (2005), Characteristics and spatio-temporal variability of the Amazon River Basin Water Budget, *Clim. Dyn.*, *24*(1), 11–22, doi:10.1007/s00382-004-0461-6.

Marengo, J. A., C. A. Nobre, J. Tomasella, M. D. Oyama, G. S. De Oliveira, R. De Oliveira, H. Camargo, L. M. Alves, and I. F. Brown (2008), The drought of Amazonia in 2005, *J. Clim.*, *21*(3), 495–516, doi:10.1175/2007JCLI1600.1.

Monteith, J. L. (1965), Evaporation and environment, *Symp. Soc. Exp. Biol.*, *19*, 205–234.

Mu, Q., F. A. Heinsch, M. Zhao, and S. W. Running (2007), Development of a global evapotranspiration algorithm based on MODIS and global meteorology data, *Remote Sens. Environ.*, *111*, 519–536, doi:10.1016/j.rse.2007.04.015.

Papa, F., C. Prigent, and W. B. Rossow (2008a), Monitoring flood and discharge variations in the large Siberian rivers from a multi-satellite technique, *Surv. Geophys.*, *29*(4–5), 297–317, doi:10.1007/s10712-008-9036-0.

Papa, F., A. Guntner, F. Frappart, C. Prigent, and W. B. Rossow (2008b), Variations of surface water extent and water storage in large river basins: A comparison of different global data sources, *Geophys. Res. Lett.*, *35*, L11401, doi:10.1029/2008GL033857.

Papa, F., C. Prigent, F. Aires, C. Jimenez, W. B. Rossow, and E. Matthews (2010), Interannual variability of surface water extent at the global scale, 1993–2004, *J. Geophys. Res.*, *115*, D12111, doi:10.1029/2009JD012674.

Prigent, C., F. Papa, F. Aires, W. B. Rossow, and E. Matthews (2007), Global inundation dynamics inferred from multiple satellite observations, 1993–2000, *J. Geophys. Res.*, *112*, D12107, doi:10.1029/2006JD007847.

Rabus, B., M. Eineder, A. Roth, and R. Bamler (2003), The shuttle radar topography mission—A new class of digital elevation models acquired by spaceborne radar, ISPRS *J. Photogramm. Remote Sens.*, *57*(4), 241–262, doi:10.1016/S0924-2716(02)00124-7.

Richey, J. E., R. H. Meade, E. Salati, A. H. Devol, C. F. Nordin, and U. Dossantos (1986), water discharge and suspended sediment concentrations in the Amazon River 1982–1984, *Water Resour. Res.*, *22*(5), 756–764, doi:10.1029/WR022i005p00756.

Roads, J., M. Kanamitsu, and R. Stewart (2002), CSE water and energy budgets in the NCEP-DOE Reanalysis II, *J. Hydrometeorol.*, *3*(3), 227–248, doi:10.1175/1525-7541(2002)003<0227:CWAEBI>2.0.CO;2.

Rodell, M., and J. S. Famiglietti (1999), Detectability of variations in continental water storage from satellite observations of the time dependent gravity field, *Water Resour. Res.*, *35*(9), 2705–2723, doi:10.1029/1999WR900141.

Rodell, M., J. S. Famiglietti, J. Chen, S. I. Seneviratne, P. Viterbo, S. Holl, and C. R. Wilson (2004), Basin scale estimates of evapotranspiration using GRACE and other observations, *Geophys. Res. Lett.*, *31*, L20504, doi:10.1029/2004GL020873.

Seo, K. W., and C. R. Wilson (2005), Simulated estimation of hydrological loads from GRACE, *J. Geod.*, *78*(7–8), 442–456, doi:10.1007/s00190-004-0410-5.

Sheffield, J., C. R. Ferguson, T. J. Troy, E. F. Wood, and M. F. McCabe (2009), Closing the terrestrial water budget from satellite remote sensing, *Geophys. Res. Lett.*, *36*, L07403, doi:10.1029/2009GL037338.

Sheffield, J., E. F. Wood, and F. Munoz-Arriola (2010), Long-term regional estimates of evapotranspiration for Mexico based on downscaled ISCCP data, *J. Hydrometeorol.*, *11*(2), 253–275, doi:10.1175/2009JHM1176.1.

Sorooshian, S., et al. (2011), Advanced concepts on remote sensing of precipitation at multiple scales, *Bull. Am. Meteorol. Soc.*, *92*, 1353–1357, doi:10.1175/2011BAMS3158.1.

Swenson, S., and J. Wahr (2006), Post-processing removal of correlated errors in GRACE data, *Geophys. Res. Lett.*, *33*, L08402, doi:10.1029/2005GL025285.

Syed, T. H., J. S. Famiglietti, J. Chen, M. Rodell, S. I. Seneviratne, P. Viterbo, and C. R. Wilson (2005), Total basin discharge for the Amazon and Mississippi River basins from GRACE and a land-atmosphere water balance, *Geophys. Res. Lett.*, *32*, L24404, doi:10.1029/2005GL024851.

Syed, T. H., J. S. Famiglietti, and D. P. Chambers (2009), GRACE-Based Estimates of Terrestrial Freshwater Discharge from Basin to Continental Scales, *J. Hydrometeorol.*, *10*(1), 22–40, doi:10.1175/2008JHM993.1.

Tang, Q. H., H. L. Gao, P. Yeh, T. Oki, F. G. Su, and D. P. Lettenmaier (2010), Dynamics of terrestrial water storage change from satellite and surface observations and modeling, *J. Hydrometeorol.*, *11*(1), 156–170, doi:10.1175/2009JHM1152.1.

Vörösmarty, C. J., C. J. Willmott, B. J. Choudhury, A. L. Schloss, T. K. Stearns, S. M. Robeson, and T. J. Dorman (1996), Analyzing the discharge regime of a large tropical river through remote sensing, ground-based climatic data, and modeling, *Water Resour. Res.*, *32*(10), 3137–3150, doi:10.1029/96WR01333.

Wahr, J., S. Swenson, V. Zlotnicki, and I. Velicogna (2004), Time-variable gravity from GRACE: First results, *Geophys. Res. Lett.*, *31*, L11501, doi:10.1029/2004GL019779.

Wang, K., R. E. Dickinson, M. Wild, and S. Liang (2010), Evidence for decadal variation in global terrestrial evapotranspiration between 1982 and 2002: 1. Model development, *J. Geophys. Res.*, *115*, D20112, doi:10.1029/2009JD013671.

Zeng, N. (1999), Seasonal cycle and interannual variability in the Amazon hydrologic cycle, *J. Geophys. Res.*, *104*(D8), 9097–9106, doi:10.1029/1998JD200088.

Zeng, N., J. H. Yoon, J. A. Marengo, A. Subramaniam, C. A. Nobre, A. Mariotti, and J. D. Neelin (2008), Causes and impacts of the 2005 Amazon drought, *Environ. Res. Lett.*, *3*(1), 014002, doi:10.1088/1748-9326/3/1/014002.

Zhang, K., J. S. Kimball, R. R. Nemani, and S. W. Running (2010), A continuous satellite-derived global record of land surface evapotranspiration from 1983 to 2006, *Water Resour. Res.*, *46*, W09522, doi:10.1029/2009WR008800.

M. Azarderakhsh, R. Khanbilvardi, and W. B. Rossow, NOAA-Cooperative Remote Sensing Science and Technology Center, City College of New York, Steinmen Hall, Convent Avenue and 140th Street, New York, NY 10031, USA. (mazarderakhsh@gc.cuny.edu)

H. Norouzi, Construction Management and Civil Engineering Technology, New York City College of Technology, 300 Jay St., New York, NY 11201, USA.

F. Papa, IRD LEGOS, 18 Avenue Edouard Belin, F-31400 Toulouse, France.